Supplementary Material: Reporting Experimental Information and Data

Mechanistic investigation of the denitrosylation activity of a water-soluble copper(II) compound probed by experimental and computational approaches

Bruna B. Segat [a], Adolfo Horn Jr.[a], Bruno Szpoganicz [a], Lino Meurer [a], Roberta Cargnelutti [b],Rodrigo Cervo [b], Luis Gabriel Wagner [a], Sreerag N. Moorkkannur Narayanan [c], Rajeev Prabhakar [c], Lucas C. Pinheiro [d], Siti Noriza Kamel [e], Sumeet Mahajan [e], Martin Feelisch [f], and Christiane Fernandes*

[a] B. B. Segat, Departamento de Química, Universidade Federal de Santa Catarina, 88040-900, Florianópolis, SC, Brazil, bruna.segat@posgrad.ufsc.br; A. Horn Jr., Departamento de Química, Universidade Federal de Santa Catarina, 88040-900, Florianópolis, SC, Brazil, adolfo.junior@ufsc.br; B. Szpoganicz, Departamento de Química, Universidade Federal de Santa Catarina, 88040-900, Florianópolis, SC, Brazil, bruno.s@ufsc.br; L. Meurer, Departamento de Química, Universidade Federal de Santa Catarina, 88040-900, Florianópolis, SC, Brazil, lino.m.l@posgrad.ufsc.br; L. G. Wagner, Departamento de Química, Universidade Federal de Santa Catarina, 88040-900, Florianópolis, SC, Brazil, luis.gabriel.wagner@hotmail.com; C. Fernandes, Departamento de Química, Universidade Federal de Santa Catarina, 88040-900, Florianópolis, SC, Brazil, christiane.horn@ufsc.br

[b] R. Cargnelutti, Departamento de Química, Universidade Federal de Santa Maria, 97105-900, Santa Maria, RS, Brazil, roberta.cargnelutti@ufsm.br; R. Cervo. Departamento de Química, Universidade Federal de Santa Maria, 97105-900, Santa Maria, RS, Brazil, rodrigo.cervo@acad.ufsm.br

[c] R. Prabhakar, Department of Chemistry, University of Miami, Coral Gables, FL 33146, USA, rpr@miami.edu; S. M. Narayanan, Department of Chemistry, University of Miami, Coral Gables, FL 33146, USA, smn101@miami.edu

[d] L. C. Pinheiro, Departamento de Farmacologia, Universidade Federal de Santa Catarina, 88040-900, Florianópolis, SC, Brazil, lucas.c.pinheiro@ufsc.br

[e] S. N. Kamel. Institute for Life Sciences, University of Southampton, Southampton, United Kingdom. Siti.Noriza.Mohd-Kamel@soton.ac.uk.

[e] S. Mahajan, [1]School of Chemistry, Faculty of Engineering and Physical Sciences, University of Southampton, and [2]Institute for Life Sciences, University of Southampton, Southampton, United Kingdom. S.Mahajan@soton.ac.uk

[f] M. Feelisch, Clinical & Experimental Sciences, Faculty of Medicine, Southampton General Hospital; and [2] Institute for Life Sciences, University of Southampton, Southampton, United Kingdom. M.Feelisch@soton.ac.uk

S1-Experimental Section

S1.1. Equipment and conditions used

The ligand HL and its copper compound **1** were synthesized using P.A grade of reagents. UV–Vis, ESI-(+)-MS and EPR investigations were carried out employing spectroscopic, HPLC or MS quality solvents. All chemicals and reagents were purchased from Merck and used as received. Infrared spectra were recorded with a Shimadzu FT-IR 8300 spectrophotometer. The ligand HL, isolated as an oil, was measured as a film on a KBr disk. A sample of compound **1** was prepared in a KBr pellet. Spectra were recorded over the range of 400–4000 cm^{-1}. Full electronic spectra were recorded using an Agilent Cary 60 UV-vis spectrometer with a thermostatted cuvette holder and quartz cuvettes, and select absorbance readings were performed on a TECAN (Infinite 200 pro) using a 96-well plate suitable for UV readings. Electron Paramagnetic Resonance (EPR) spectra were obtained using a Bruker EMX micro-9.5/2.7/P/L system using a highly sensitive cylindrical cavity, operating in X-band (~9.5 GHz), with 5 mW microwave power, 5 G modulation amplitude and 100 kHz modulation frequency. The spectra were simulated using SpinFit and Anisospin softwares provided by the manufacturer (Bruker). The experiments were carried out at 100 K or 295 K, as indicated in the Figures. Full scan mass spectra (MS mode) were obtained on an Electrospray Ionization (ESI-MS) AmaZon X Ion Trap mass spectrometer (Bruker Daltonics, Germany), in positive mode, ion-source voltage of 4500 V, flow injection or flow rate of 180 μL/h, nebulizing gas (0.4 bar) and dry gas (4 L min^{-1}), ion-source temperature 180 and 200°C and the scan range was *m/z* 100–2000. Single-crystal X-ray diffraction data were obtained with a Bruker D8 Venture diffractometer equipped with a Photon 100 detector, Incoatec microfocus Montel optic X-ray tube with Mo-Kα radiation (λ = 0.71073Å). The structure was solved and refined with the SHELX program package.[1,2] Non-hydrogen atoms were refined anisotropically. The molecular structure was drawn with the Diamond program.[3] The crystallographic information file (CIF) for compound **1** was deposited at the Cambridge Crystallographic Data Centre (CCDC) under identification number 2320978. These data can be obtained free of charge via http://www.ccdc.cam.ac.uk/conts/retrieving.html (or from the Cambridge Crystallographic Data Centre, 12, Union Road, Cambridge CB2 1EZ, UK;

fax: +44 1223 336033). •NO quantifications were obtained using a water-jacketed glass reaction chamber connected to an Eco Medics CLD 88 sp detector with N_2 gas or synthetic air as carrier gas. Surface Enhanced Raman Spectroscopy (SERS) measurement was performed with a Renishaw InVia confocal Raman microscope (λ = 785 nm) equipped with a 50x long working distance objective (Olympus, NA 0.5) and a 1200 lines/mm grating. Acquisitions typically used 0.5 mW laser power, 1s acquisition time and 3 accumulations.

S1.2. Synthesis of ligand HL and characterization of compound 1

The syntheses and the characterization of the ligand (HL) and the compound $[Cu(HL)Cl_2]$ **1** (Scheme 1) have been described in our previous studies. [4,5]

Compound **1** was obtained through a reaction between the ligand HL1 (1 mmol, 152 mg) and $CuCl_2{\cdot}2H_2O$ (1 mmol, 170 mg) in methanol, resulting in a blue microcrystalline solid. Yield: 230mg (82%). m.p.: 175°C. Anal. Calcd for $C_8H_{12}Cl_2CuN_2O$; MW = 286.64g.mol^{-1}: C, 33.52; H, 4.21; N 9.77. Found: C, 33.66; H, 4.19; N, 9.60.

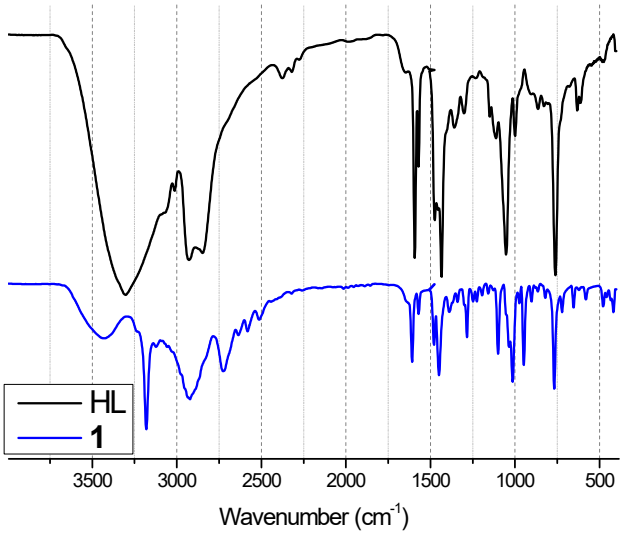

Figure 1S. Infrared spectra obtained for the ligand HL (black line) and its copper(II) compound **1** (blue line)**.**

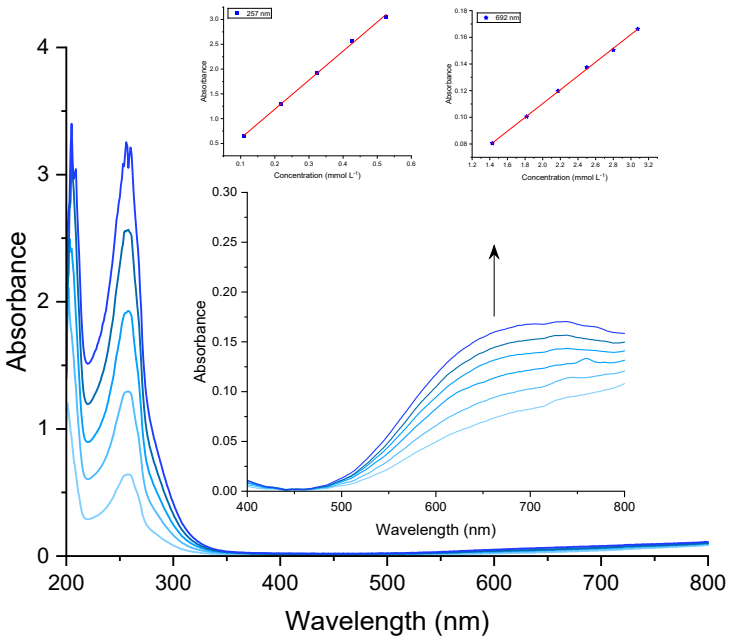

Figure 2S. Electronic spectra of compound **1** at different concentrations, obtained in PBS buffer. λ 257 nm (π→π* of ligand, ε = 5859 mol L^{-1} cm^{-1}), λ 692 nm (d→d, ε = 51.8 mol L^{-1} cm^{-1}).

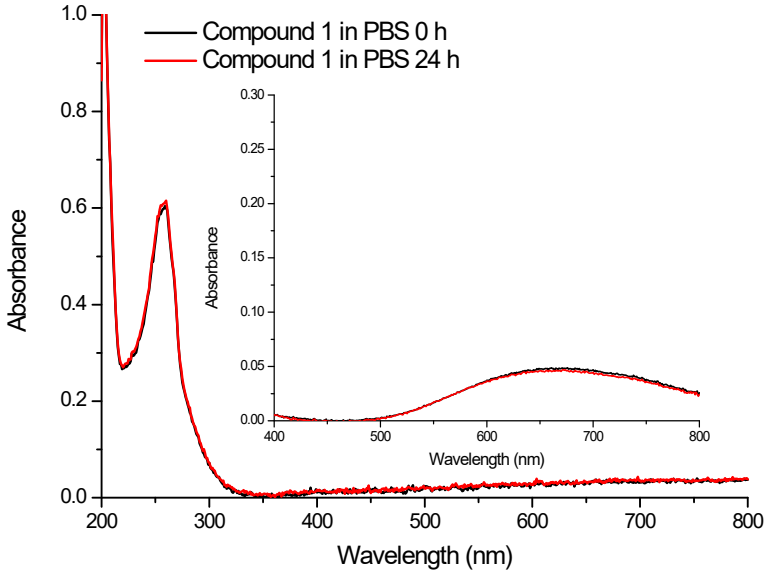

Figure 3S. Stability of compound **1** in PBS at 37ºC, monitored by electronic spectroscopy. Concentration of **1**: 100 µmol L^{-1}, inset: 1 mmol L^{-1}. Essentially identical results were obtained at RT (not shown).

Table 1S. Crystallographic and refinement data for compound **1**.

Formula	$C_8H_{12}Cl_2CuN_2O$
F.W. ($g \cdot mol^{-1}$)	286.64
Crystal system	Monoclinic
Space group	$P2_1/n$
a (Å)	7.8503(18)
b (Å)	9.7175(13)
c (Å)	14.293(4)
α (°)	90
β (°)	94.735(10)
γ (°)	90
T (K)	298(2)
V ($Å^3$)	1086.6(4)
Z	4
$r_{calc.}$ ($g \cdot cm^{-3}$)	1.752
μ (mm^{-1})	2.469
F(000)	580
Reflections collected	13174
Independent reflections	3315 [R(int) = 0.0202]
R_1 *[I > 2σ(I)]*	0.0224
wR_2 [I > 2σ(I)]	0.0582
R_1 (all data)[a]	0.0261
wR_2 (all data)[b]	0.0604
GOOF on F^2	1.082
Largest diff. peak and hole ($e.Å^{-3}$)	0.323 and -0.574

[a]$R_1 = \sum||F_o|-|F_c||/\sum|F_o|$; [b]$wR_2 = \{\sum w(F_o^2-F_c^2)^2/\sum w(F_o^2)^2\}^{½}$

Table 2S. Main bond distances (Å) and angles (°) for compound **1**.

Bond lengths (Å)		Angles (°)	
Cu1–N1	1.9943(12)	N1–Cu1–N2	82.75(5)
Cu1–N2	2.0127(12)	N1–Cu1–O1	158.32(5)
Cu1–O1	2.0244(11)	N2–Cu1–O1	82.48(5)
Cu1–Cl1	2.2430(5)	N1–Cu1–Cl1	98.92(4)
Cu1–Cl2	2.6135(6)	N2–Cu1–Cl1	167.58(3)
O1–C8	1.4423(18)	O1–Cu1–Cl1	92.26(3)

N1–C5	1.3436(17)	N1–Cu1–Cl2	103.11(4)
N1–C1	1.3450(18)	N2–Cu1–Cl2	93.54(4)
N2–C6	1.4733(17)	O1–Cu1–Cl2	93.56(4)
N2–C7	1.4772(18)	Cl1–Cu1–Cl2	98.027(19)

1

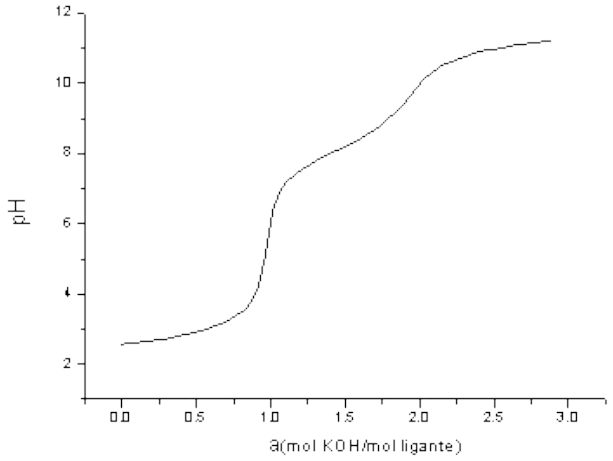

2

3 **Figure 4S.** Potentiometric titration curve of the ligand HL, at 25.0 ºC and μ= 0.1 mol L^{-1}
4 (KCl).

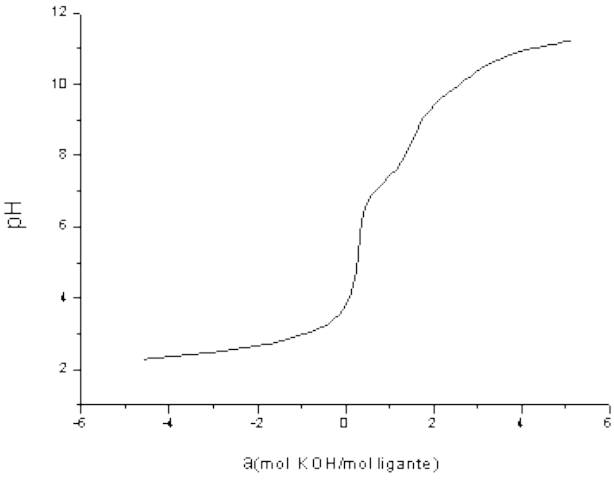

5

6 **Figure 5S.** Potentiometric titration curve of compound **1**, at 25.0 ºC and μ= 0.1 mol L^{-1}
7 (KCl).

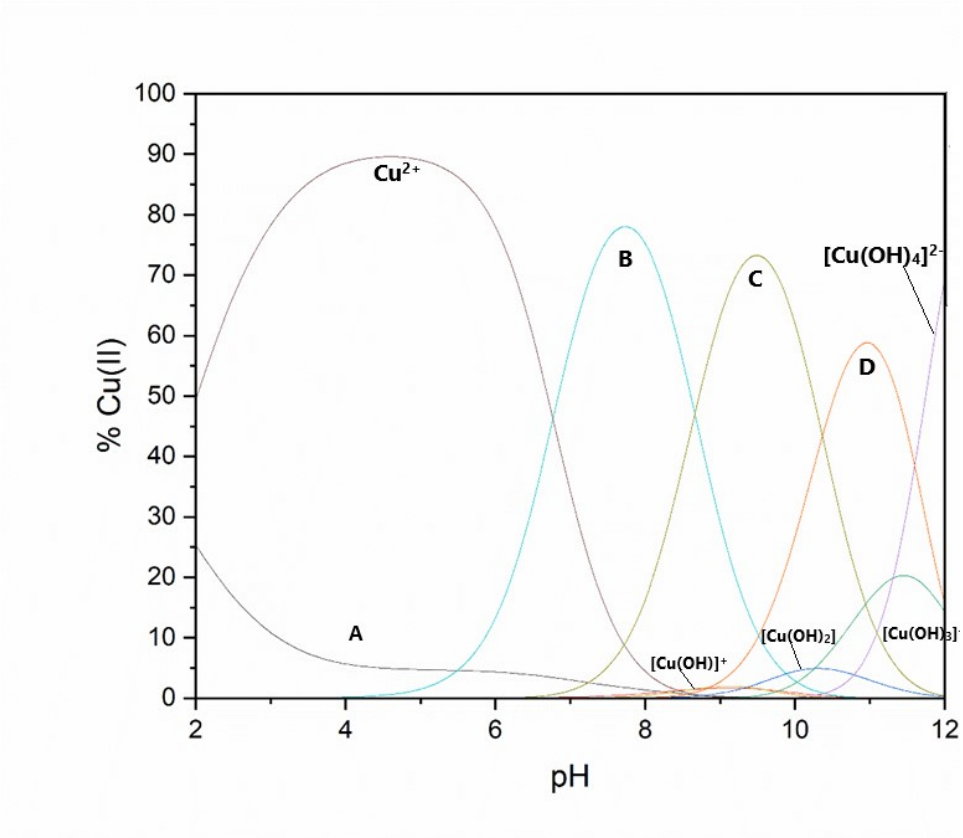

Figure 6S. Distribution of copper species in solution, in function of pH, where A = $[Cu(H_2L)(OH_2)_2]^{3+}$, B = $[Cu(HL)(OH_2)_2]^{2+}$, C = $[Cu(L)(H_2O)_2]^{+}$, D = $[Cu(L)(H_2O)(OH)]$.

Table 3S. Species present in solution at each pH, according to potentiometric titration.

Quotient	Log K
$CuHLCl_2$	
$A/B[H^+]$	6.52
$B/C[H^+]$	8.39
$C/D[H^+]$	10.30
Ligand HL	
$[L][H^+]/[HL^+]$	8.09

A = $[Cu(H_2L)(OH_2)_2]^{3+}$, B = $[Cu(HL)(OH_2)_2]^{2+}$, C = $[Cu(L)(OH_2)_2]^{+}$, D = [Cu(L) (OH_2) (OH)].

S3- Investigation of the denitrosylation of GSNO promoted by compound 1

S3.1. Compound 1 induced GSNO denitrosylation as assessed by electronic spectroscopy- *in vitro* studies

A 20 mmol L^{-1} stock solution of GSNO was prepared by mixing 1 volume of 40 mmol L^{-1} aqueous solution of sodium nitrite ($NaNO_2$) with 1 volume of a 40 mmol L^{-1} aqueous solution of GSH at RT. The yield of GSNO obtained by this method was compared with the standard procedure of GSNO synthesis, which uses acidified $NaNO_2$ solution. The yield of GSNO produced was identical (Figure 7S). For the stability studies, 25 µL of the 20 mmol L^{-1} GSNO stock was added to a 96-well plate. The experiment was performed in triplicate. To each well of the triplicate, 25 µL of a 5.0 mmol L^{-1} solution of compound **1**, prepared in PBS, was added. The volume was adjusted to 250 µL with PBS. Absorbance readings were taken at a fixed wavelength of 335 nm, on a TECAN (Infinite 200 pro) plate reader immediately after plating and after 1h incubation at 37 °C. Sodium ascorbate (Asc) and copper chloride ($CuCl_2$) were used as controls due to their known capacity to remove the •NO group from nitrosothiols.[6] The absorbance of GSNO alone was considered to represent 100% nitrosation.

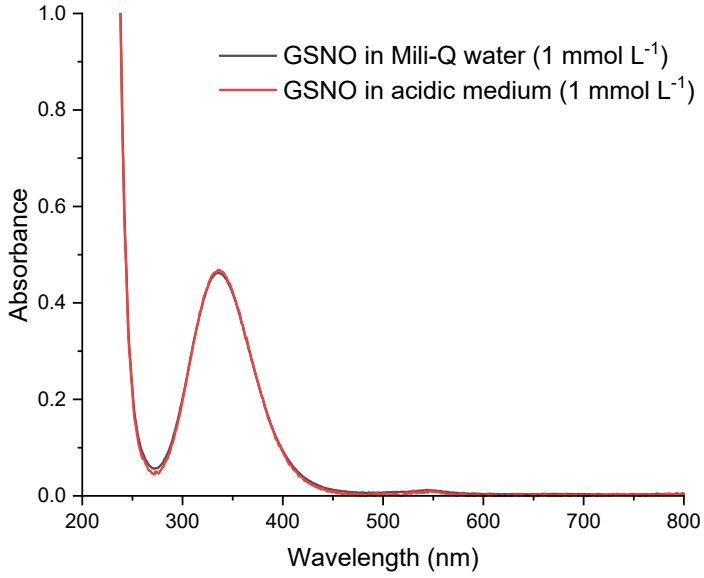

Figure 7S. Electronic spectra of GSNO obtained by the standard method, with acidified $NaNO_2$ solution (red line) and by the method used in this paper, in Milli-Q water (black line).

For full electronic spectra acquisition 100 µL of a 100 µmol L^{-1} solution of compound **1** prepared in PBS (0.01 mol L^{-1}) were added to a 1 mmol L^{-1} GSNO solution prepared by diluting the 20 mmol L^{-1} aqueous solution in PBS (0.01 mol L^{-1}). Readings were performed from 200 to 800 nm every 2 min (GSNO:1 proportion of 10:1). 100 µL of a 25 µmol L^{-1} solution of complex **1** prepared in PBS (0.01 mol L^{-1}) was added to a 1 mmol L^{-1} GSNO solution prepared by diluting the 20 mmol L^{-1} aqueous solution in PBS (0.01 mol L^{-1}). Readings were performed from 200 to 800 nm every 10 min (GSNO:1 proportion of 40:1).

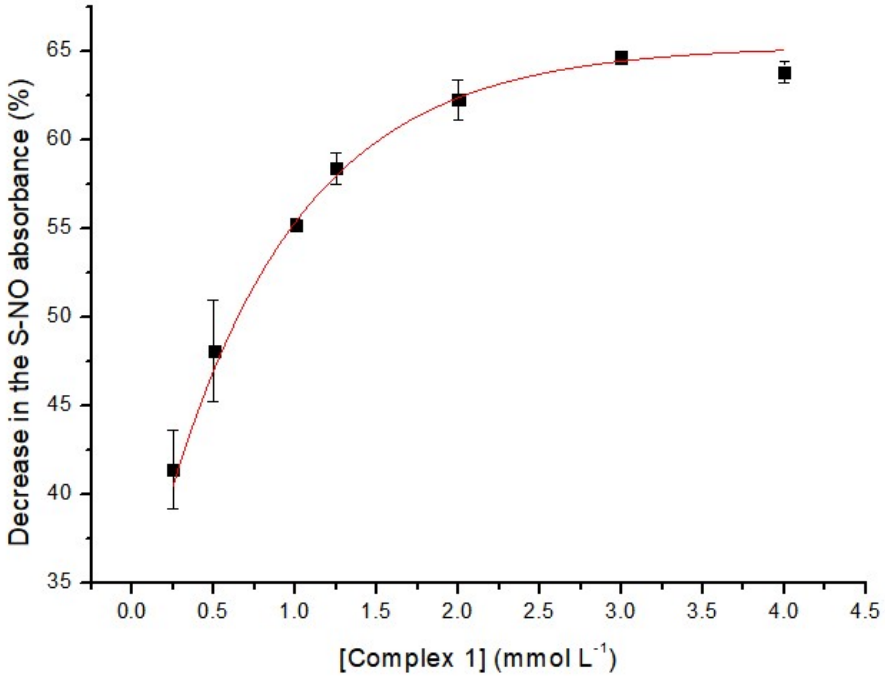

Figure 8S. Exponential fitting of the decrease in absorbance at 335 nm, attributed to the S-NO transition, against the concentration of compound **1**. Initial concentration of GSNO = 2 mmol L^{-1}. Concentrations of **1**: 0.25, 0.5, 1.0, 1.25, 2, 3 and 4 mmol L^{-1}.

S 3.2-Kinetic studies of the interaction between compound 1 and GSNO

25 µL of a 100 µmol L^{-1} solution of compound **1,** in PBS (0.01 mol L^{-1}), were injected to a 96-well plate containing 225 µL of different concentrations of an aqueous solution of GSNO (concentrations varying between 1 and 5 mmol L^{-1}, with a 0.25 mmol L^{-1} increase between each point) (Table 4S). The readings were performed every 30 s

for 30 min at the fixed wavelength of 335 nm. The initial velocity method was applied, and the Hill model was used to fit the curve obtained.[7]

Table 4S. Initial velocities obtained for each concentration of GSNO during kinetic studies. Absorbance at 335 nm was monitored every 30 s for 30 min. Compound **1** concentration of 100 μmol L^{-1}.

[GSNO] mmol L^{-1}	**Slope**	**R^2**
1.0	1.87E-04 (±9.53962E-06)	0.9981 (±0.0004)
1.25	2.10E-04 3.12748E-06)	0.9956 (±0.0017)
1.5	2.78E-04 (±1.86875E-05)	0.9882 (±0.0014)
1.75	3.26E-04 (±2.32512E-05)	0.9978 (±0.0009)
2.0	3.30E-04 (±1.26834E-05)	0.9991 (±0.0003)
2.25	3.73E-04 (±1.17377E-05)	0.9990 (±0.0003)
2.5	4.08E-04 (±3.75648E-06)	0.9991 (±0.0001)
2.75	4.48E-04 (±2.90593E-06)	0.9986 (±0.0003)
3.0	4.24E-04 (±1.24677E-05)	0.9963 (±0.0005)
3.25	4.73E-04 (±2.66667E-06)	0.9983 (±0.0006)
3.5	4.99E-04 (±2.11765E-05)	0.9981 (±0.0007)
3.75	4.96E-04 (±5.696E-06)	0.9976 (±0.0004)
4.0	4.96E-04 (±2.4173E-06)	0.9973 (±0.0004)
4.25	4.66E-04 (±1.15662E-05)	0.9964 (±0.0005)
4.5	4.88E-04 (±4.37163E-06)	0.9931 (±0.0006)
4.75	4.67E-04 (±5.48736E-06)	0.9944 (±0.0012)
5.0	4.86E-04 (±2.16744E-05)	0.9944 (±0.0017)

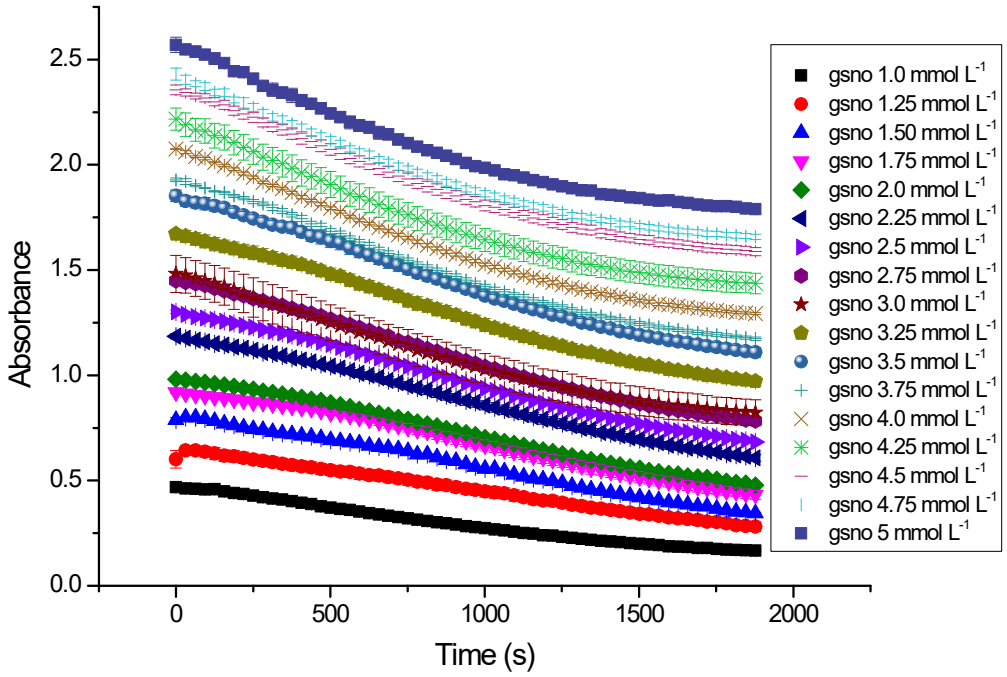

Figure 9S. Non-normalized kinetic data of the interaction between compound **1** and GSNO.

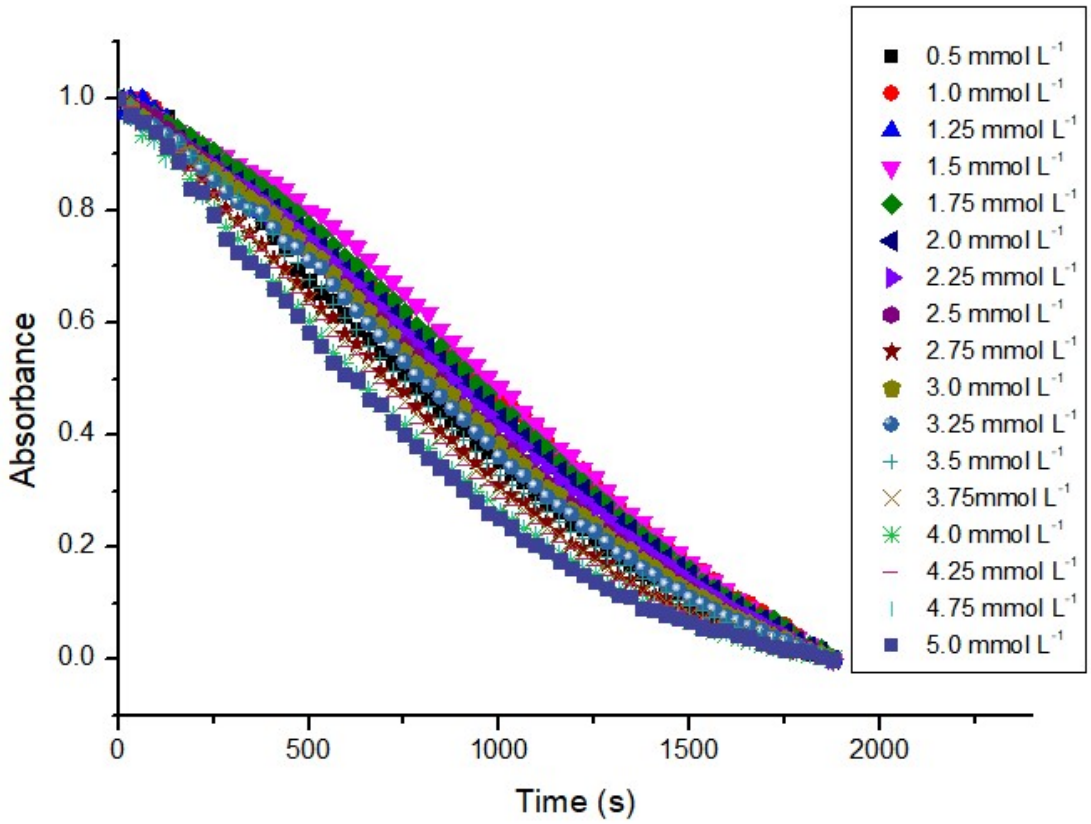

Figure 10S. Normalized decrease in the absorbance at 335 nm through time using different concentrations of GSNO. Readings were performed every 30 s. Compound **1** concentration used was 0.1 mmol L^{-1}.

S3.3-EPR studies of the interaction between compound 1 and GSNO

EPR studies of the interaction between GSNO and **1** were performed at 100 K, using 4 mm quartz tubes. 50 uL of a 4 mmol L^{-1} solution of **1**, prepared in PBS was mixed with 50 uL of different concentrations of a GSNO aqueous solution and 100 uL of PBS (0.1 mol L^{-1}). The different concentrations of GSNO were obtained by diluting a 40 mmol L^{-1} stock solution of GSNO, which was obtained by mixing equimolar solutions of GSH and $NaNO_2$ as described above. In the experiments related to the reactions between **1** and GSNO, the solutions were frozen after 3 min of reaction.

EPR studies of the interaction between **1** and GSNO employing DMPO as spin trapping were performed at room temperature (295 K), using a capillary tube. The DMPO was used to detect additional radical species possibly formed during the reaction. 50 µL of a 4 mmol L^{-1} solution of **1,** prepared in PBS were mixed with 50 µL

of a 400 mmol L^{-1} solution of DMPO, prepared in Mili-Q water, 50 µL of a 40 mmol L^{-1} GSNO aqueous solution, and 50 µL of PBS (0.1 mol L^{-1}).

To spin quantification, we conducted experiments in open air or under an argon atmosphere using a glove bag. Utilizing Schlenk glassware, solutions of compound **1** and GSNO were subjected to a vacuum and purged with argon for five cycles. After this, the solutions were handled inside the glove bag. The reactions (300 µL) were then transferred to EPR tubes, which were capped, and after 3 min, frozen in liquid nitrogen.

The •NO release was studied using the system presented in Figure 12S.

Reactionbetween complex **1** and GSNO was performed by mixing 400 µL of a 4 mmol L^{-1} solution of complex **1** (prepared in PBS) with 400 µL of a 40 mmol L^{-1} aqueous solution of GSNO. A 10 mmol L^{-1} solution of $[Fe(DETC)_2]$ was prepared in DMSO to serve as •NO scavenger. The system was closed right after the addition of the solution of GSNO into the solution containing **1**. A sample of the $[Fe(DETC)_2]$ solution was collected after 5 min, and its EPR spectrum was measured. A similar investigation was carried out employing a similar Zn(II) complex $[Zn(HL)Cl_2]$, which was previously reported by us. Reference 4 is already cited at the end of the supplementary material.

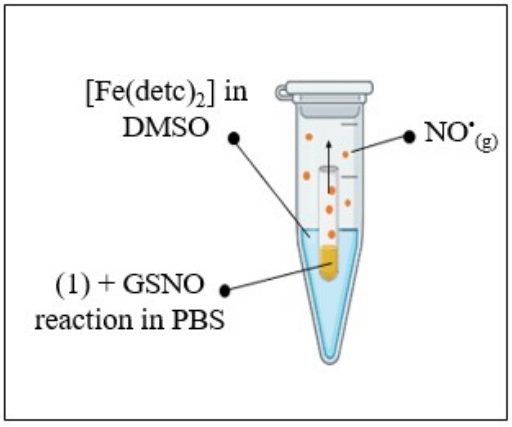

Figure 11S. The system used for the EPR evaluation of the release of gaseous •NO by the reaction between 4 mmol L^{-1} of compound **1**, in PBS, and 4 mmol L^{-1} of GSNO, in water. GSNO was prepared by mixing equimolar solutions of GSH and $NaNO_2$ in water. A 10 mmol L^{-1} solution of ferrous-diethyldithiocarbamate $[Fe(DETC)_2]$ was prepared in DMSO to serve as a •NO scavenger. The system was closed right after the addition of the solution of GSNO into the solution containing compound **1,** and an

aliquot of the [Fe(DETC)$_2$] containing solution was collected. The EPR spectrum was obtained after 5 min.[8]

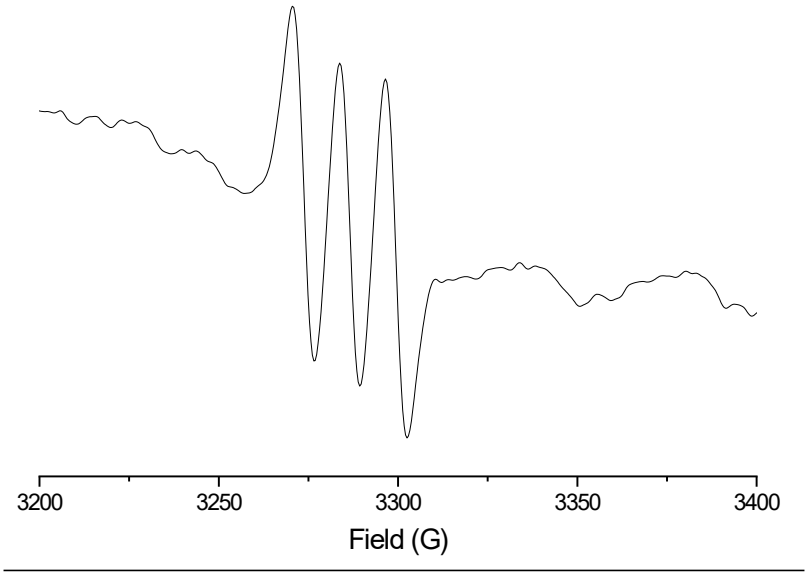

Figure 12S. Experimental EPR spectra obtained in the reaction of [Fe(DETC)$_2$] (in DMSO) with gaseous •NO generated from the reaction of GSNO and the Zn(II) compound [Zn(HL)Cl$_2$], in PBS buffer/DMSO, T = 293 K.

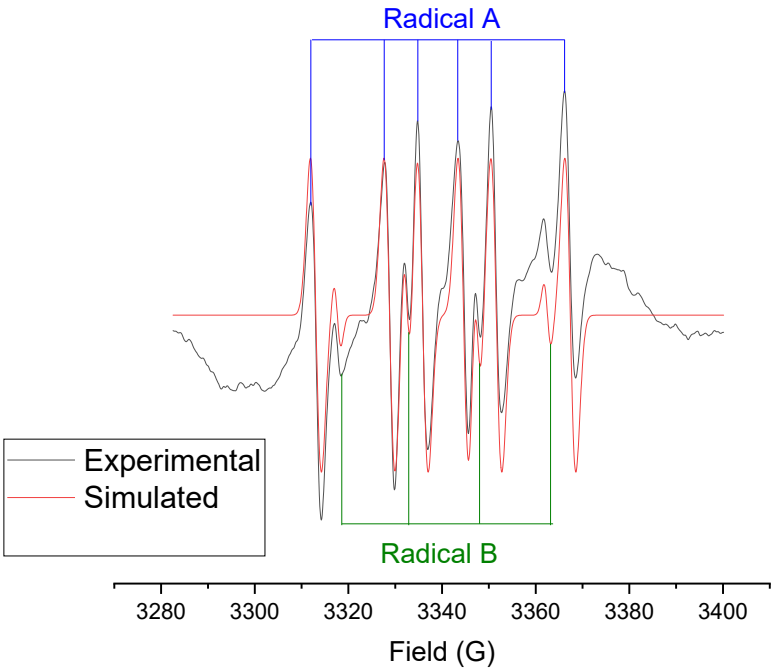

1

2 **Figure 13S.** EPR spectrum of the reaction between **1** and GSNO in the presence of the
3 spin trap DMPO. The experimental spectrum (black) was simulated (red) considering the
4 presence of two different radical species: radical A A_N = 15.768 G and A_H = 22.8098) and
5 radical B (A_N = 15.147 G and A_H = 14.6118 G).

6

7

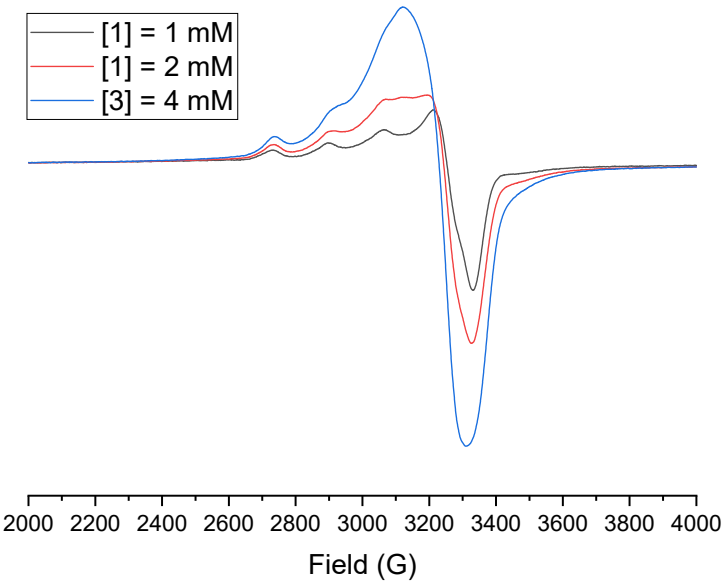

1

2 **Figure 14S.** EPR spectra of compound **1** at different concentrations, in PBS, as
3 indicated, at 100 K.

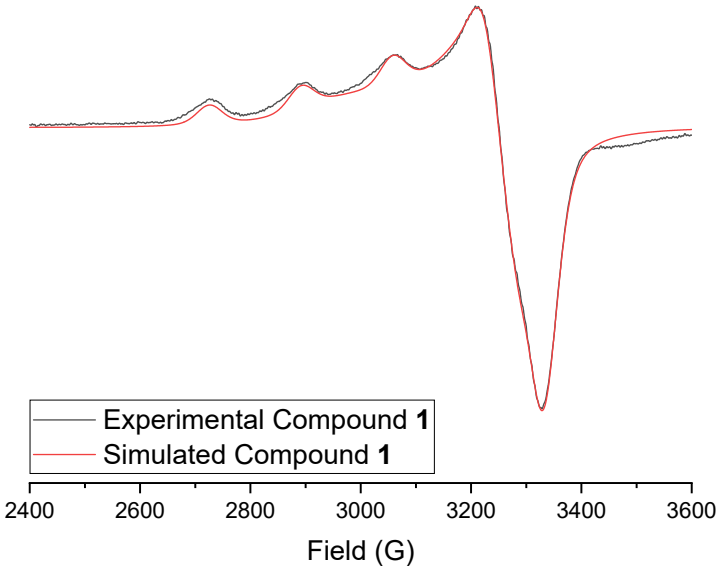

4

5 **Figure 15S.** Experimental and simulated EPR of compound **1**, at 1 mM, in PBS, at 100
6 K

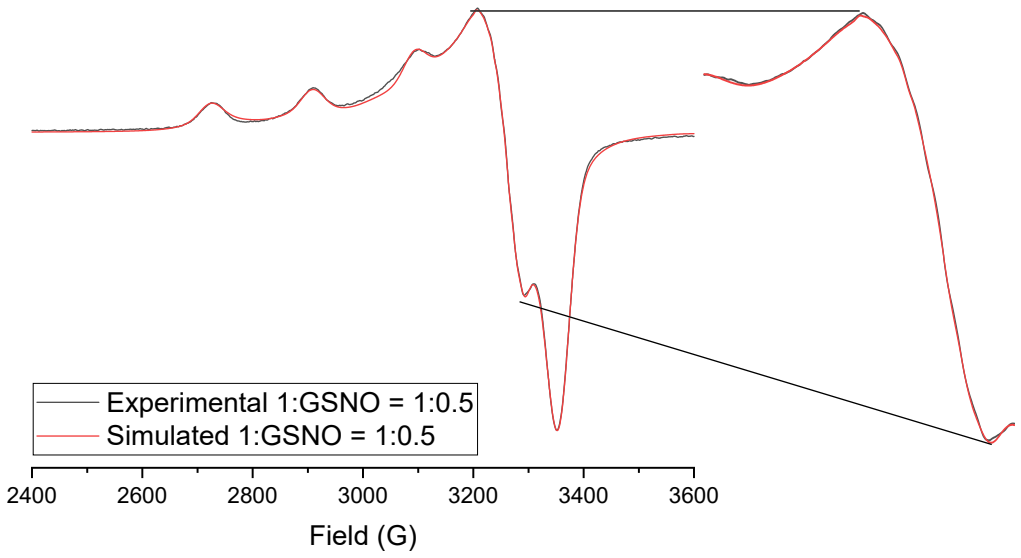

Figure 16S. Experimental and simulated EPR spectra of a PBS solution containing compound **1** and GSNO, at a ratio of 1:0.5. The enlarged area allows tracking the super-hyperfine splitting, better visualized at higher GSNO concentration.

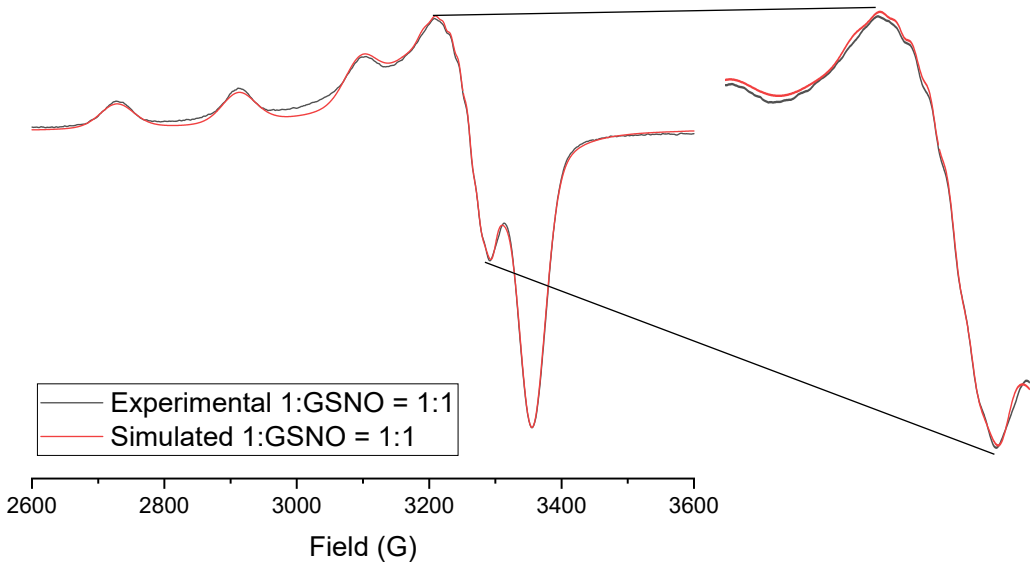

Figure 17S. Experimental and simulated EPR spectra of a PBS solution containing compound **1** and GSNO, at a ratio of 1:1. The enlarged area allows tracking the super-hyperfine splitting, better visualized at higher GSNO concentration.

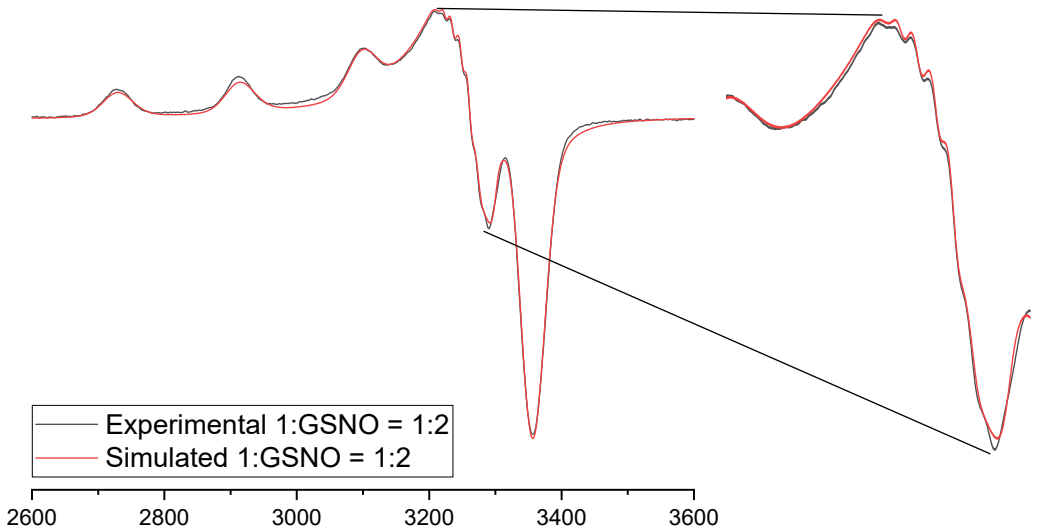

Figure 18S. Experimental and simulated EPR spectra of a PBS solution containing compound **1** and GSNO, at a ratio of 1:2. The enlarged area allows tracking the super-hyperfine splitting, better visualized at higher GSNO concentration.

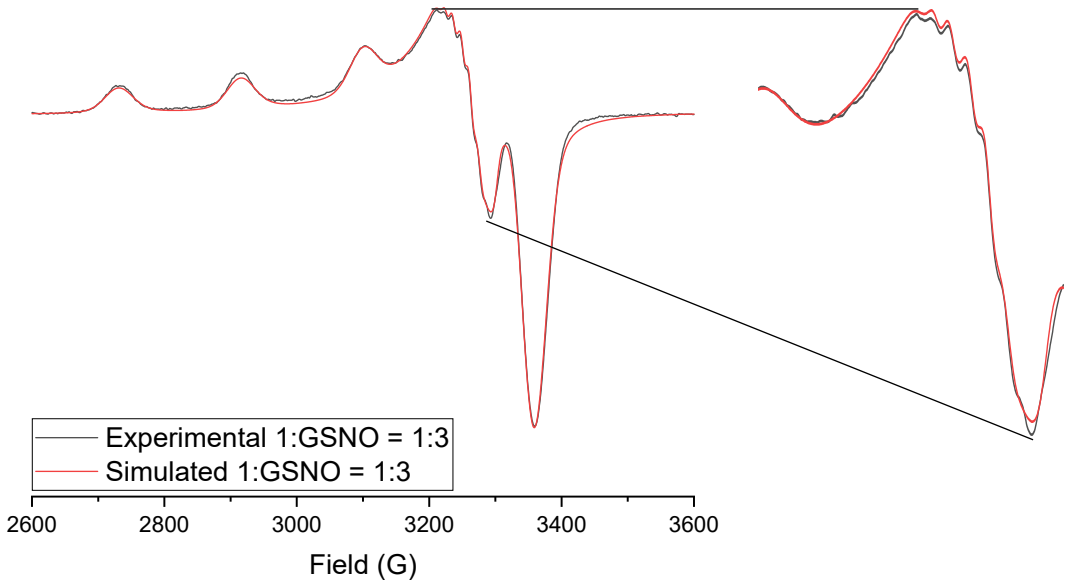

Figure 19S. Experimental and simulated EPR spectra of a PBS solution containing compound **1** and GSNO, at a ratio of 1:3. The enlarged area allows tracking the super-hyperfine splitting, better visualized at higher GSNO concentration.

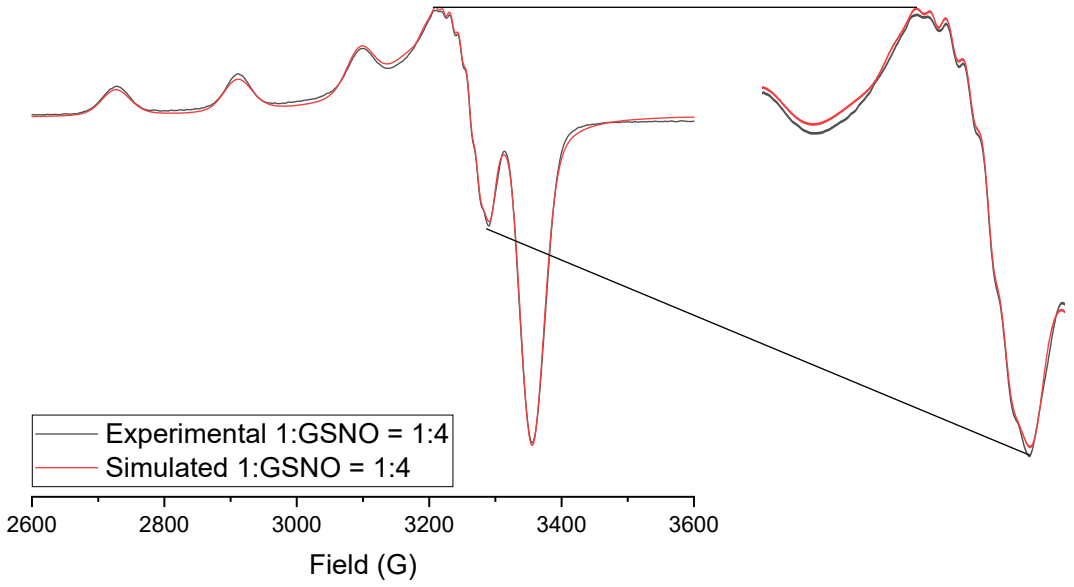

1

2 **Figure 20S.** Experimental and simulated EPR spectra of a PBS solution containing
3 compound **1** and GSNO, at a ratio of 1:4. The enlarged area allows tracking the super-
4 hyperfine splitting, better visualized at higher GSNO concentration.

Table 5S. EPR parameters obtained by simulating the experimental spectra (Figures 13S-18S) acquired from a PBS solution, at 100K, using various ratios of compound **1** (1.0 mM) to GSNO (as indicated).

Species	EPR parameter	Ratio **1**:GSNO **Copper Center** **1:0**	**1:0.5**	**1:1**	**1:2**	**1:3**	**1:4**
species Cu_A	g_x (LW[a])	2.0583(76.8)	2.0643(39.1)	2.0809(61)	2.0702(50.5)	2.0674(50.6)	2.0703(54.8)
	g_y(LW)	2.0434(37.8)	2.0333(35.2)	2.0367(34)	2.0364(32.3)	2.0367(33.4)	2.0371(32.4)
	g_z(LW)	2.2501(44.7)	2.2315(40)	2.2300(48)	2.2279(41.8)	2.2283(39.8)	2.2300(38.8)
	A_x x 10^4 cm	18.4	15.6	18.7	20.6	20.9	26.0
	A_y x 10^4 cm	19.1	23.4	17.7	28.5	21.5	28.0
	A_z x 10^4 cm	156	172	172	172	172	172
	Weight[b]	62535	69756	113399	112791	69943	126281
Species Cu_B	g_x (LW[a])	2.0694(140)	2.0785(163)	-	-	-	-
	g_y(LW)	2.0451(71)	2.0540(44.6)	-	-	-	-
	g_z(LW)	2.2556(167)	2.2589(101.5)	-	-	-	-
	A_x x 10^4 cm	0	0	-	-	-	-
	A_y x 10^4 cm	0	0	-	-	-	-
	A_z x 10^4 cm	0	137	-	-	-	-
	Weight[b]	40072	69880	-	-	-	-

Continuation Table 5S

		Ratio **1**:GSNO					
		System showing super-hyperfine coupling					
Species	EPR parameter	**1:0**	**1:0.5**	**1:1**	**1:2**	**1:3**	**1:4**
Species C	g_x (LW[a])		2.0461(19.7)	2.03545(10.8)	2.0346(10)	2.0346(10)	2.03538(11.5)
	g_y(LW)		2.04743(9.2)	2.05069(9.8	2.04968(10)	2.04968(10)	2.05064(10.2)
	g_z(LW)		2.05217(16)	2.07159(9.3)	2.07033(9.6)	2.07033(9.6)	2.07195(9.8)
	A_x x 10^4 cm		10.9	4.3	4.1	4.1	4.0
	A_y x 10^4 cm		3.3	5.2	5.0	4.9	5.0
	A_z x 10^4 cm		16.3	6.5	6.9	6.9	7.0
	Weight[b]		968	3384	3905	2417	4903
Species D	g_x (LW)		2.0764(9.3)	2.0637(9.3)	2.0650(5.5)	2.0650(5.5)	2.0641(6.8)
	g_y(LW)		2.0764(4.4)	2.0796(18.3)	2.0788(28)	2.0788(28)	2.0842(15)
	g_z(LW)		2.0809(4.2)	2.0749(14.2)	2.0716(15)	2.0716(15.2)	2.0710(9.8)
	A_x x 10^4 cm		0.93	12.1	11.7	11.7	12.3
	A_y x 10^4 cm		7.8	12.4	13.9	13.9	12.6
	A_z x 10^4 cm		8.1	7.2	11.6	11.6	11.9
	Weight[b]		25	1701	1253	770	1465

[a] The numbers in brackets represent the width line.[b] Represent the amount used by the program to fit the experimental spectra.

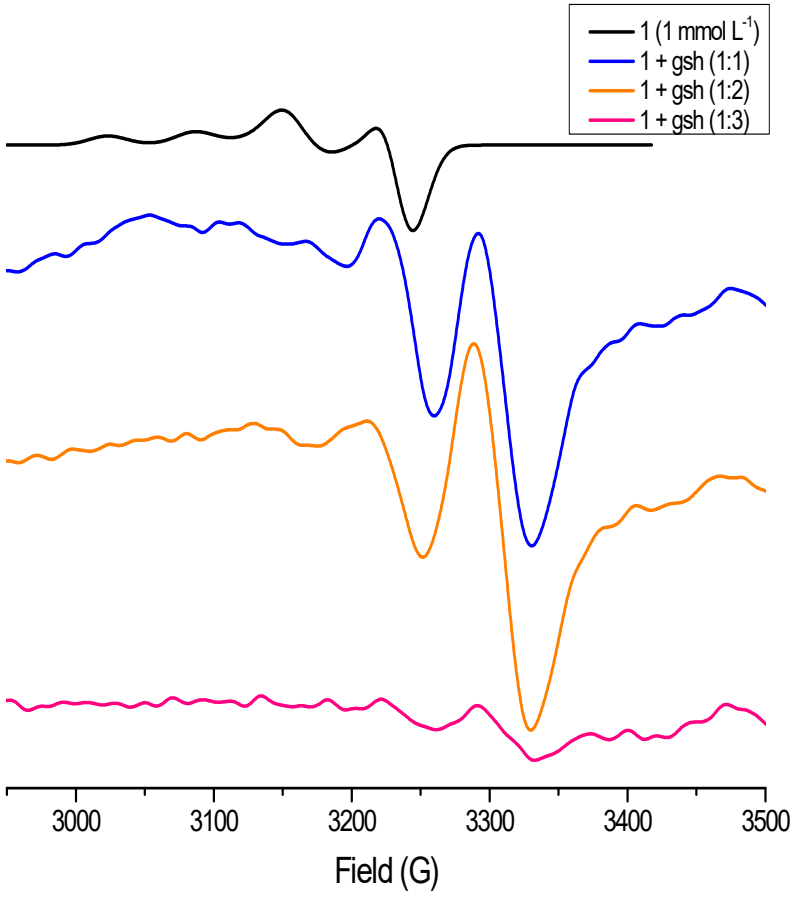

1

2 **Figure 21S.** EPR spectra, in PBS solution, at 298K, of the interaction between compound
3 **1**, initial concentration of 1 mmol L^{-1} (black), and GSH at a molar ratio of 1:1 (blue), 1:2
4 (orange), and 1:3 (pink).

1

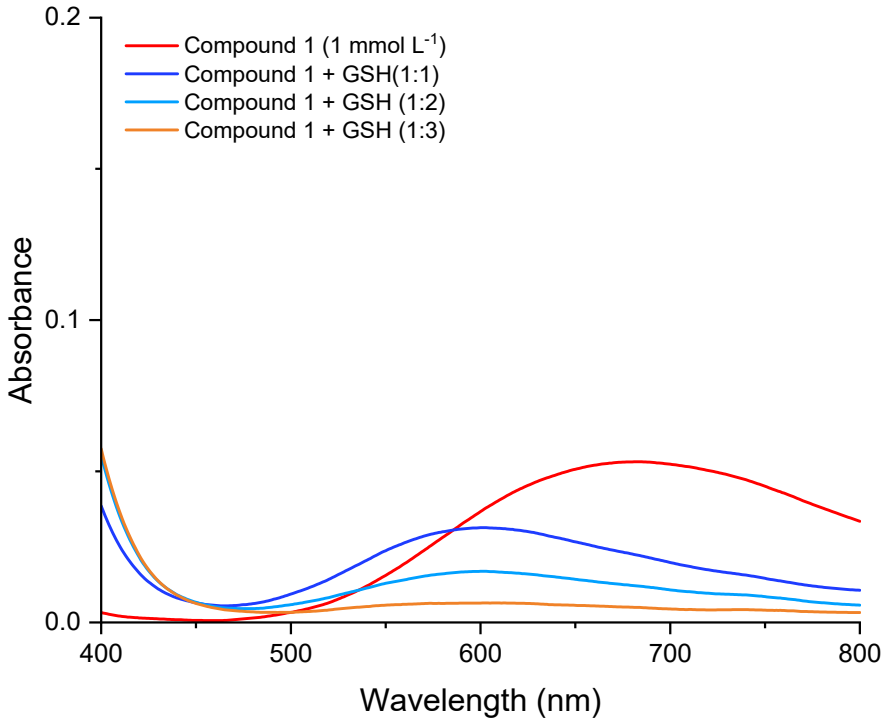

2

3 **Figure 22S.** Electronic spectra of the interaction between compound **1** (initial
4 concentration 1 mmol L^{-1}; red line) and GSH at a molar ratio of 1:1 (dark blue), 1:2
5 (light blue) and 1:3 (orange). The experiment was performed by successive 50 µL
6 additions of a 20 mmol L^{-1} solution of GSH to the cuvette containing the compound **1**
7 solution. Maximum volume added: 150 µL, The volume employed causes minimal
8 dilution effect on d-d the absorption band of compound **1** (ε = 51.8 mol L^{-1} cm^{-1})

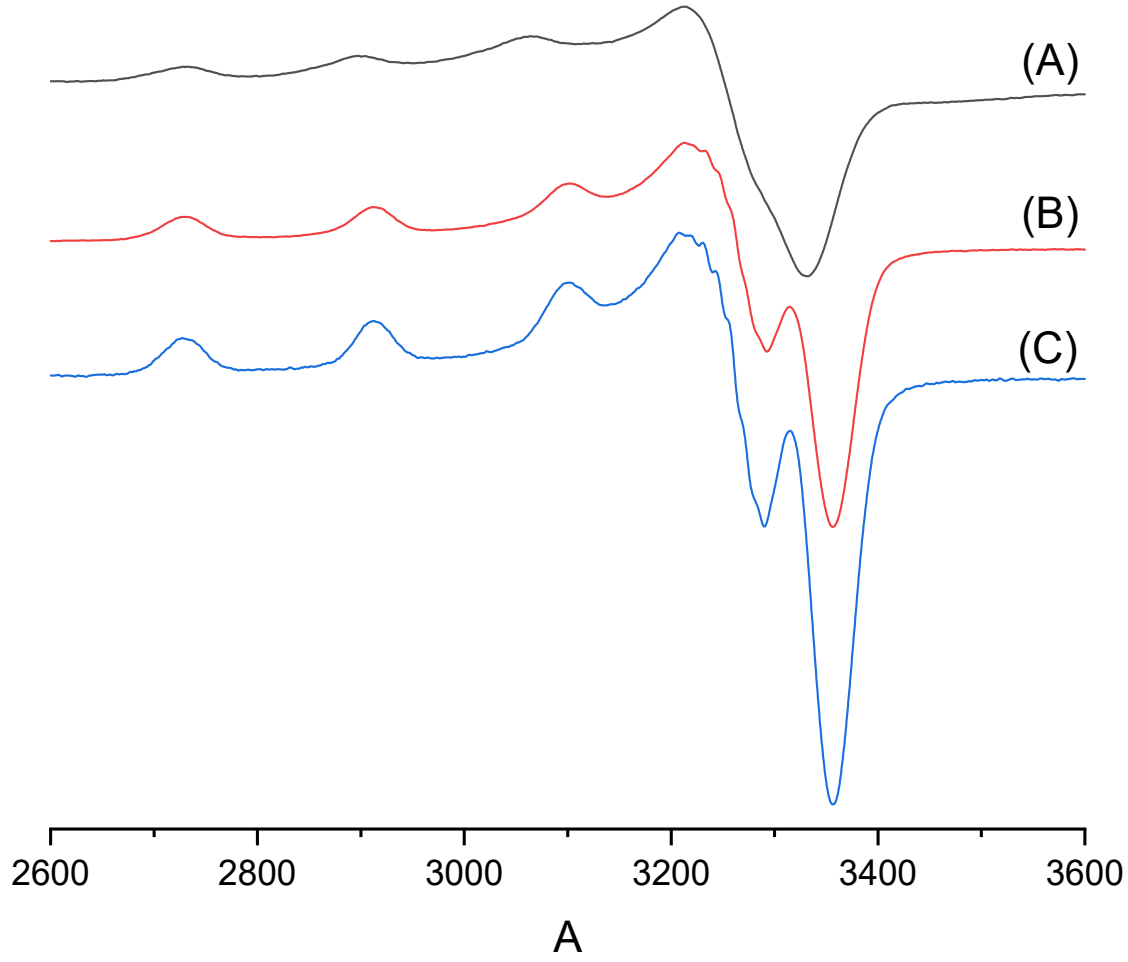

Figure 23S. EPR spectra, in PBS solution, at 100K, of: (A) compound **1**, (B) compound **1** + GSSG, (C) compound **1** + GSNO (C). [1] = 1mM, [GSSG] = 2 mM, [GSNO] = 2 mM.

S3.4- •NO release quantification by CLD (Chemiluminescence Detection) of the interaction between compound 1 and GSNO

The reaction was performed in a glass chamber under inert atmosphere (N_2) or synthetic air, and the liberation of •NO was monitored by chemiluminescence detection. The reaction chamber was filled with 11 mL of PBS buffer (0.01 mol L^{-1}). Using a Hamilton syringe, 10 µL of **1** (100 µmol L^{-1}) was added to the reaction chamber, followed by the addition of 10 µL of GSNO (1 mmol L^{-1}). The reaction was also performed by incubating a 1 mmol L^{-1} solution of GSNO with a 100 µmol L^{-1} solution of compound **1** in an Eppendorf under normal room air atmosphere and injecting 20 µL aliquots to the

reaction chamber at different time points with a Hamilton syringe. The same experiment was performed under an inert atmosphere. The stock solutions and solvents (PBS and Mili-Q water) were placed in an ultrasonic bath for 10 min for degassing prior to bubbling with Argon. All glassware and Eppendorf tubes used were filled with Argon before incubation.

Since the studies showed no significant difference between the reactions performed under normal and inert atmospheres, the experiments with copper chelators were performed under normal atmospheric conditions. 1 mmol L^{-1} solutions of neocuproine and bathocuproine were prepared in Mili-Q water. Compound **1** was incubated with both copper chelators at 10% concentration for 10 min before incubation with GSNO under the same conditions described above.

The CLD experiments were performed by incubating a GSNO solution with compound **1** in the presence and absence of bathocuproine and neocuproine, under identical conditions and at the same time. At selected time points, 20 µL aliquots from each reaction were injected into the CLD chambers. As shown in Figure 25S, the initial amount of ·NO released in the reaction incubated with chelators (Figure 25Sb) is significantly higher than that observed for the copper complex alone (Figure 25Sa), indicating a faster reaction in the presence of bathocuproine and neocuproine. Subsequent ·NO release is lower, consistent with most of the ·NO having already been released, and GSNO being denitrosylated.

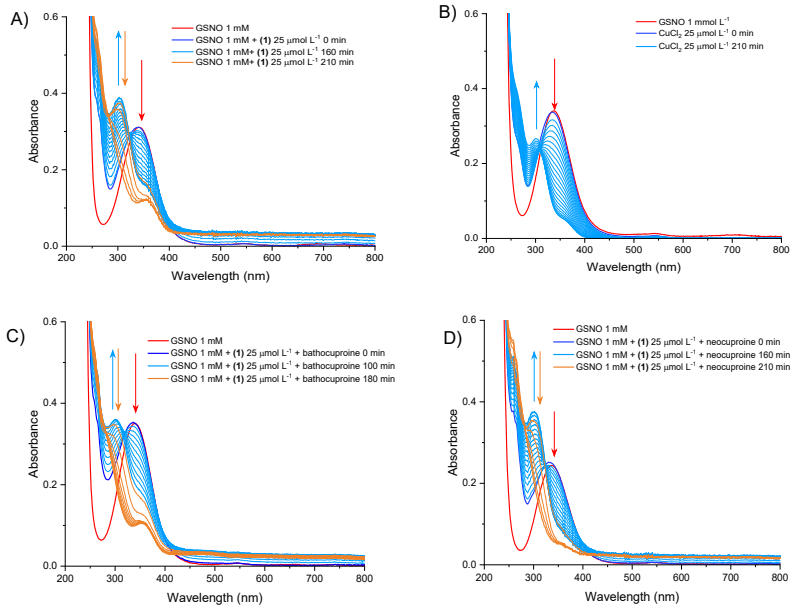

Figure 24S. Kinetic studies of the interaction between A) compound **1** and GSNO, B) $CuCl_2$ and GSNO, C) compound **1** and GSNO, in the presence of the copper chelator bathocuproine, and D) compound **1** and GSNO, in the presence of the copper chelator neocuproine. Initial GSNO concentration: 1.5 mmol L^{-1}. Compound **1** and $CuCl_2$ concentration: 25 µmol L^{-1}. For the copper chelators studies, the compound solution was incubated with each copper chelator at 10% concentration for 5 min before the addition of GSNO.

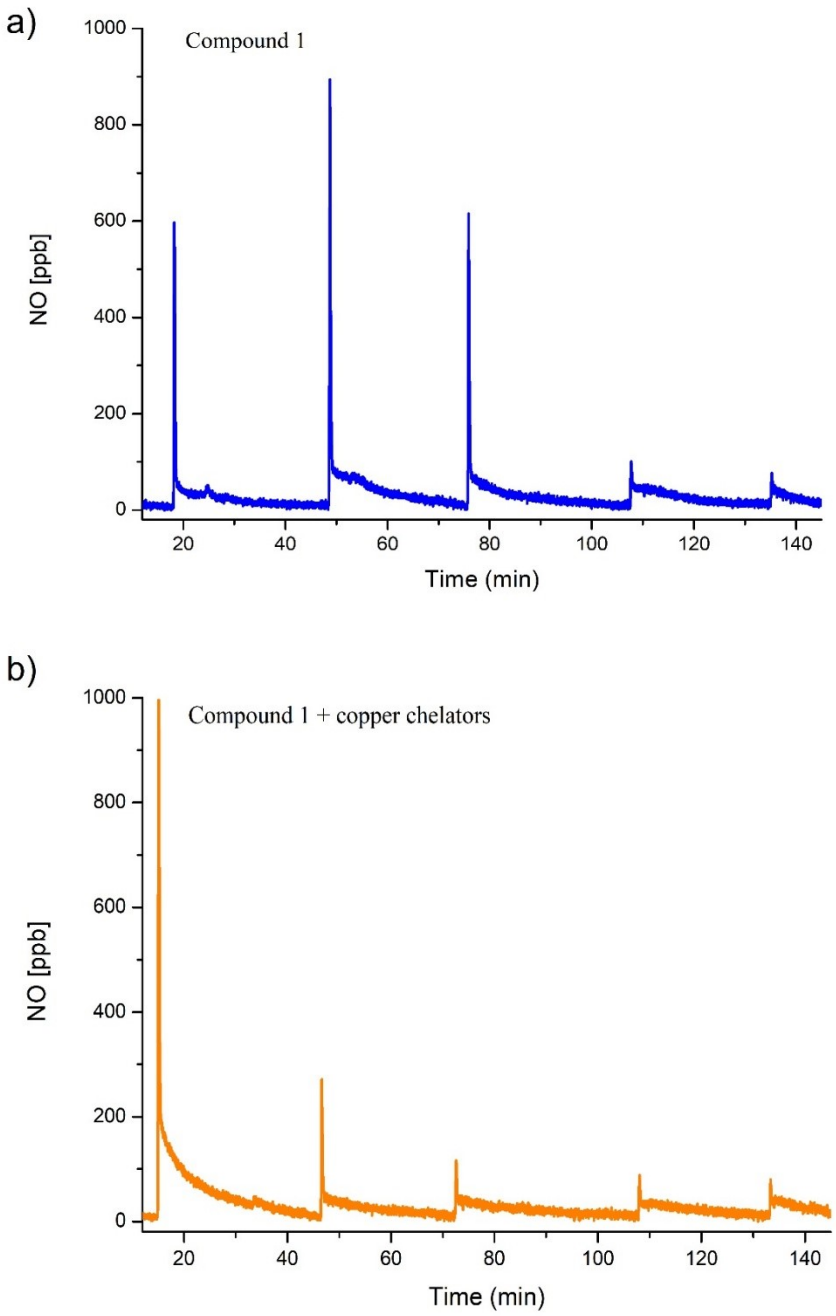

Figure 25S. a) CLD chromatogram for the reaction between **1** and GSNO. b) CLD chromatogram for the reaction between **1** and GSNO in the presence of bathocuproine and neocuproine at 10% concentration. A solution of GSNO (1 mmol L^{-1}) was incubated with a 100 µmol L^{-1} solution of compound **1**, with or without the presence of copper chelators. 20 µL aliquots of each reaction were injected into the chamber containing 13 mL of PBS at different time points. The reactions were performed under

normal atmospheric conditions, and N_2 (g) was used as the carrier gas. The amount of $^{\bullet}NO$ released is the amount of $^{\bullet}NO$ remaining in the solution after incubation.

S3.5- Surface-enhanced Raman spectroscopy (SERS) studies of the interaction between compound 1 and GSH, GSNO, and GSSG

10 mmol L^{-1} stock solutions of **1**, GSH, GSNO, and GSSG were prepared in Mili-Q water, diluted to 0.1 mmol L^{-1}, and used as controls. Spectra of the reaction between compound **1** and GSNO at a molar ratio of 1:1 and 1:2 were also obtained. 100 uL of a 0.2 mmol L^{-1} solution of **1** was added to 100 uL of a 0.2 mmol L^{-1} (1:1) and 0.4 mmol L^{-1} (1:2) solution of GSNO. A small drop of each control and reaction solution was placed on a gold-coated glass slide, and spectra were acquired in the range of 200 to 3500 cm^{-1}, using a 765 nm laser, at 0.5% laser power and 10 s exposure time.

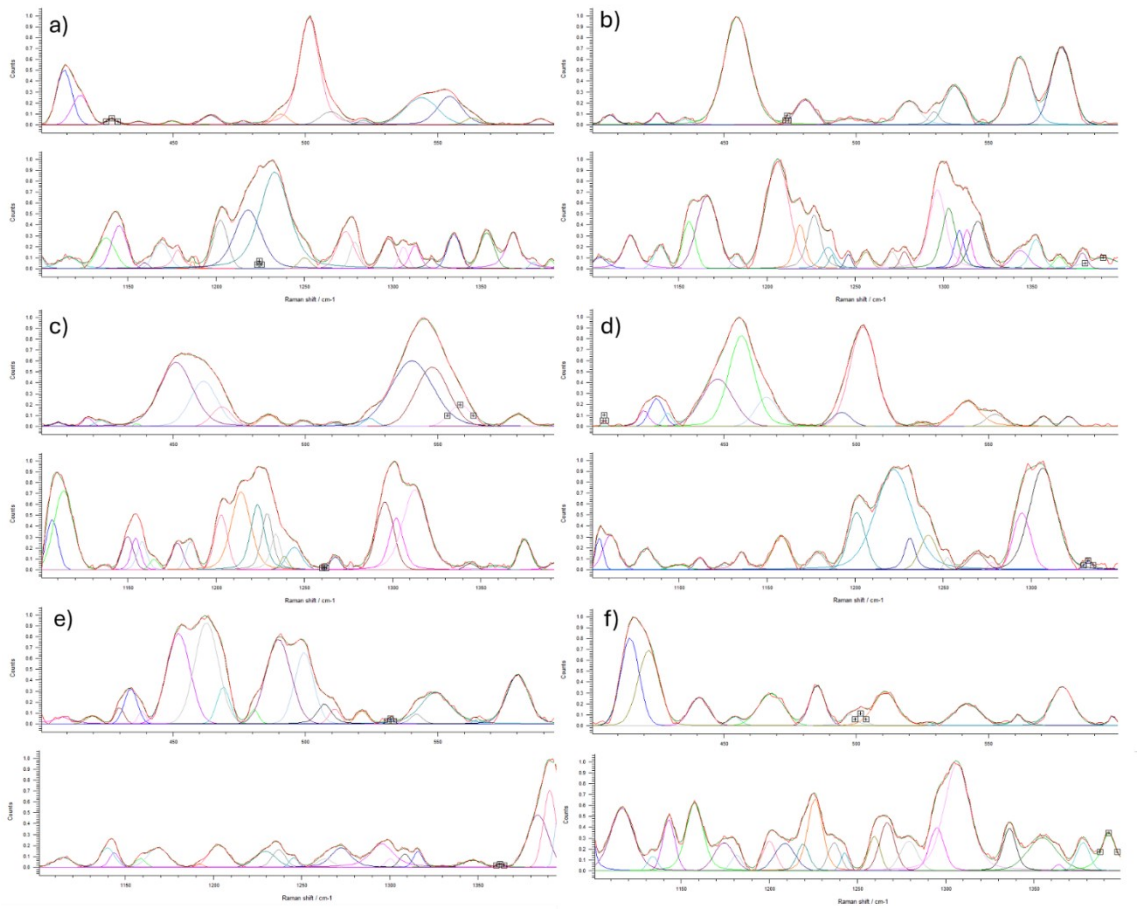

Figure 26S. Deconvolution of the SERS spectra of a) GSH, b) GSSG, c) GSNO, d) Compound **1** + GSNO (1:1), e) Compound **1** + GSNO (1:2), and f) Compound **1**.

S3.6. ESI(+)-MS/MS studies of the interaction between compound 1 and GSNO

Stock solutions were prepared in water HPLC grade. A 40 mmol L^{-1} aqueous solution of sodium nitrite ($NaNO_2$) was added to a 40 mmol L^{-1} aqueous solution of GSH, forming a 20 mmol L^{-1} solution of GSNO. The solution was diluted to 1 mmol L^{-1} and reacted with a 100 µmol L^{-1} aqueous solution of compound **1**. The reaction solution was diluted 10 times, and formic acid 0.01% was added. The reaction was then injected into the equipment using a Hamilton syringe.

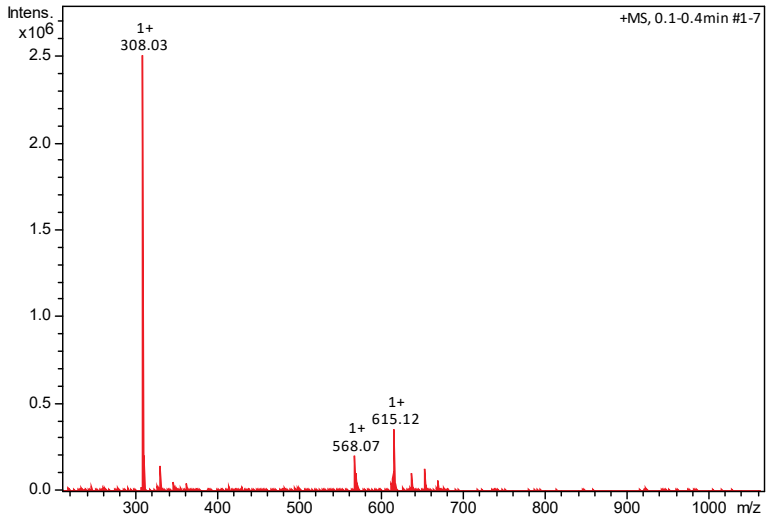

Figure 27S. Experimental ESI-(+)-MS isotopic pattern of GSH, base peak at *m/z* 308.03 corresponds to the protonated species of the molecule GSH, in water: $[GSH + H]^+$.

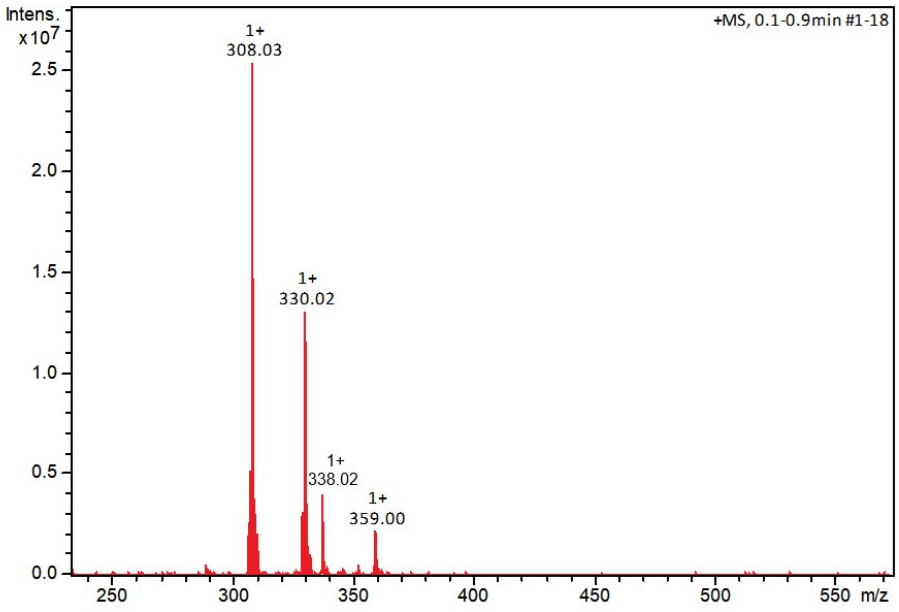

Figure 28S. Experimental ESI-(+)-MS isotopic pattern of GSNO, base peak at *m/z* 308.03 corresponds to the protonated species of the molecule GSH, and thepeak at *m/z* 338.02 corresponds to the protonated species of the molecule GSNO, in water: [GSNO + H]$^+$.

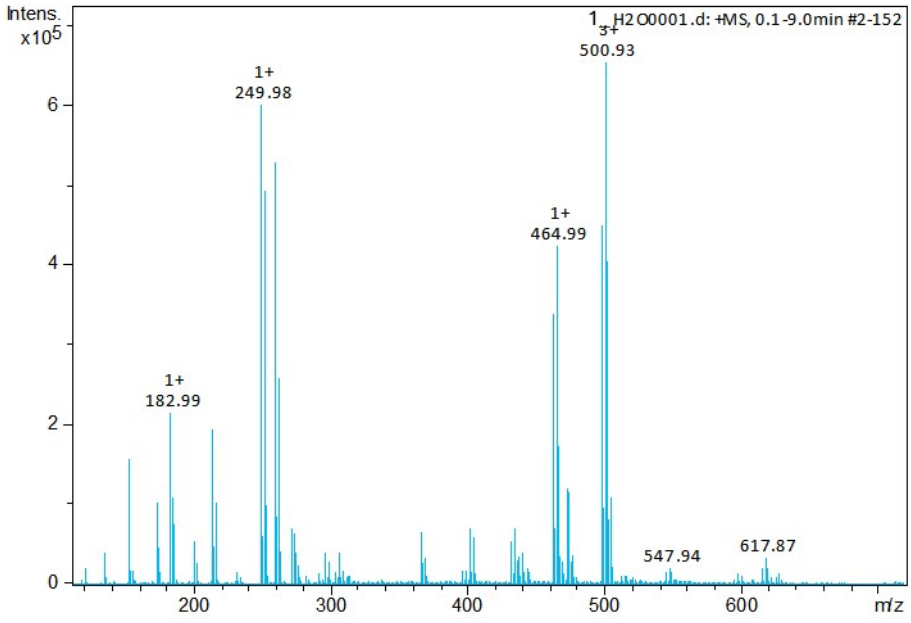

Figure 29S. Experimental ESI-(+)-MS isotopic pattern of compound **1.** Peak at *m/z* 249.98 = [Cu(HL)Cl]$^+$ and the signal at *m/z* = 500.93 = [$Cu_2(L)_2Cl$]$^+$.

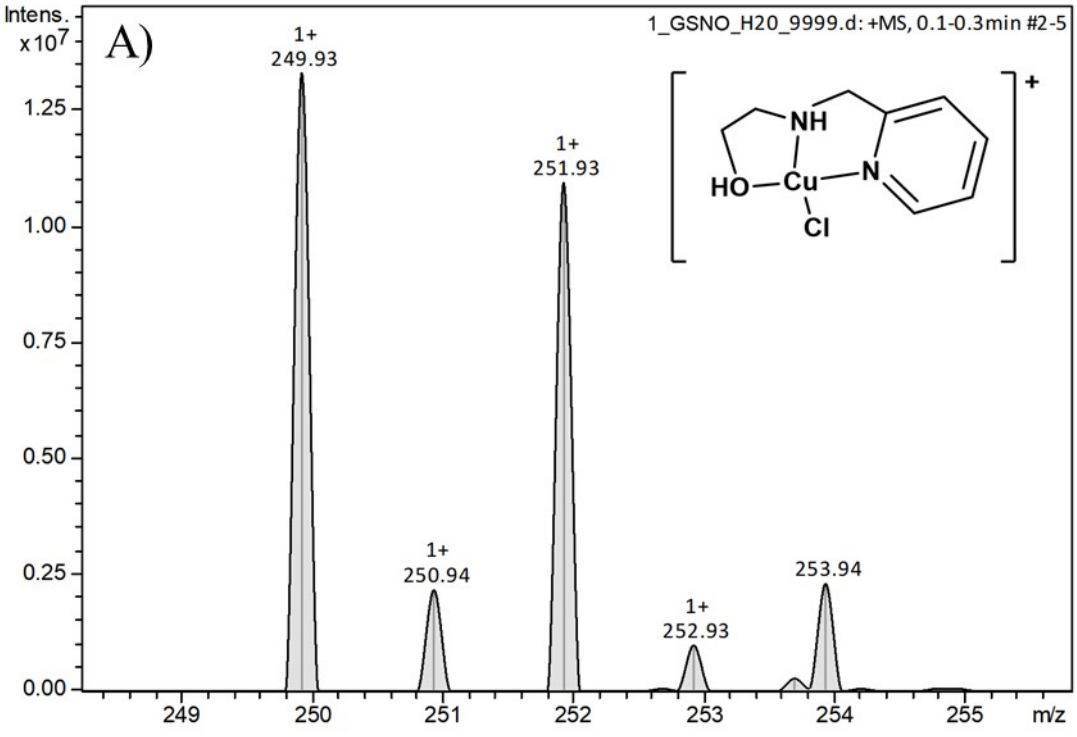

1

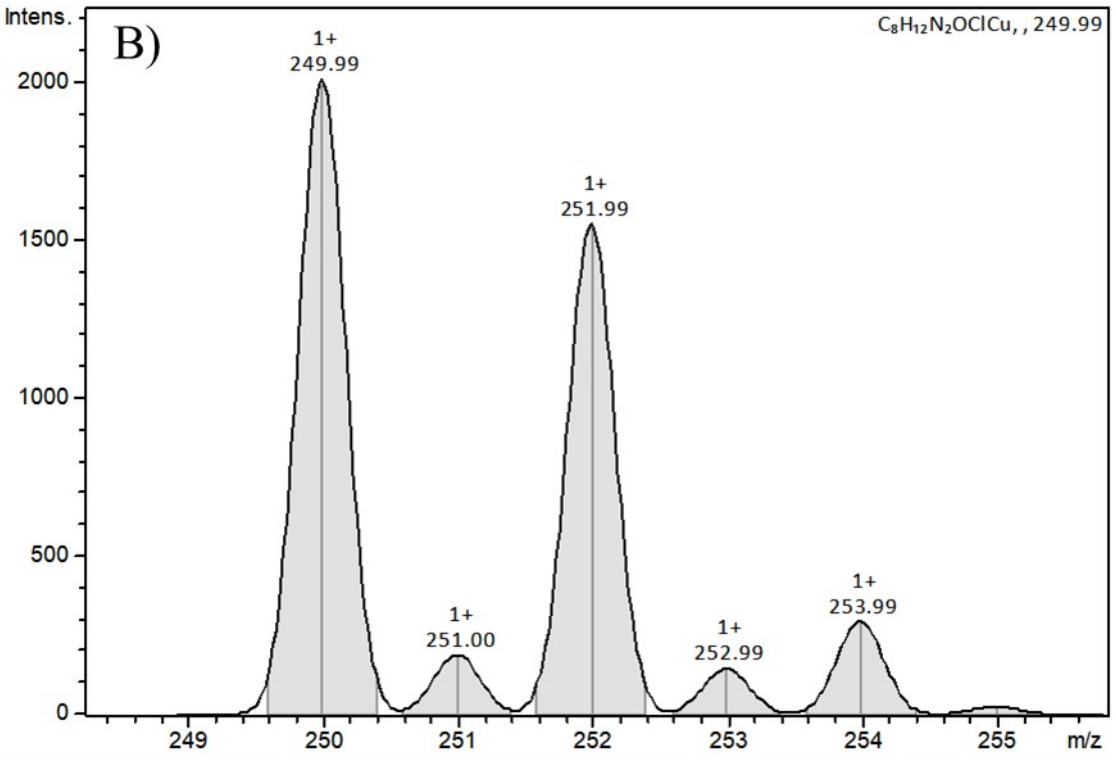

2

3 **Figure 30S.** (a) Experimental and (b) simulated ESI-(+)- MS isotopic pattern of the
4 fragment of *m/z* 249.9, corresponding to the cation $[Cu(HL)Cl]^+$

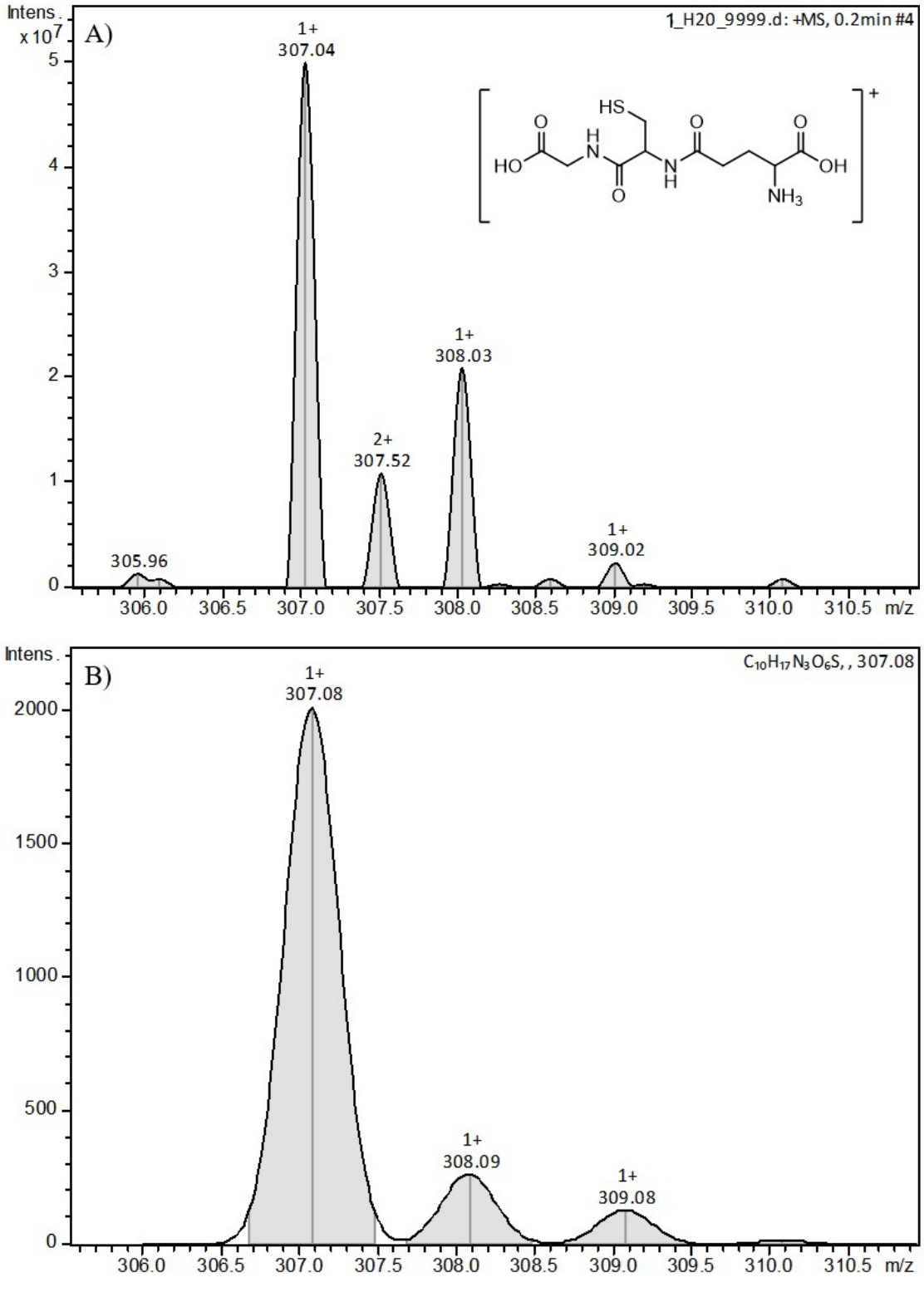

Figure 31S. Experimental and (b) simulated ESI-(+)-MS isotopic pattern of the fragment *m/z* 308.03, corresponding to protonated species of molecule GSH: $[GSH + H]^+$

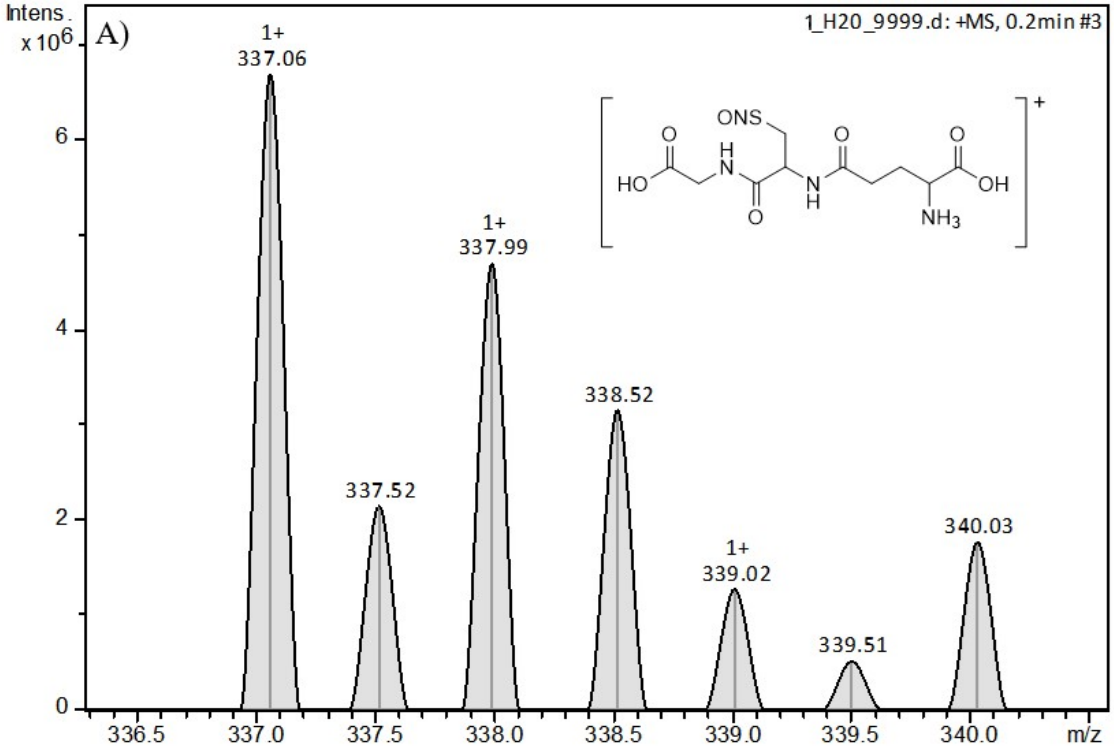

1

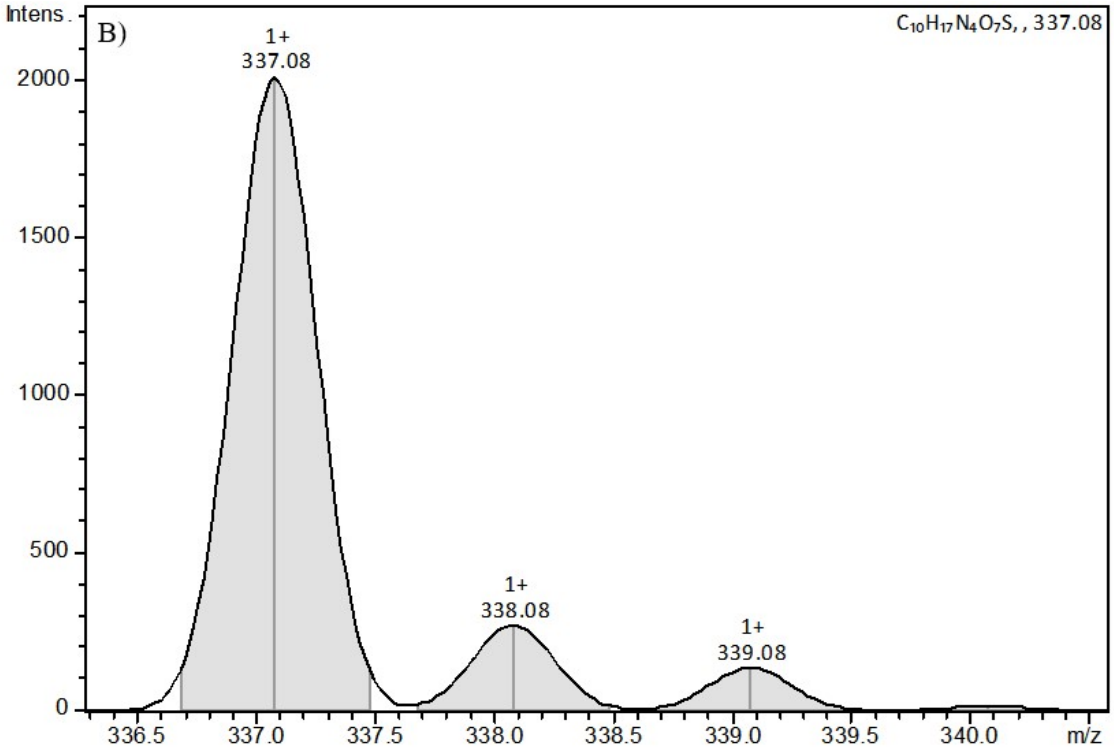

2

3 **Figure 32S.** Experimental and (b) simulated ESI-(+)-MS isotopic pattern of the
4 fragment *m/z* 338.06, corresponding to the protonated species of molecule GSNO:
5 $[GSNO + H]^+$.

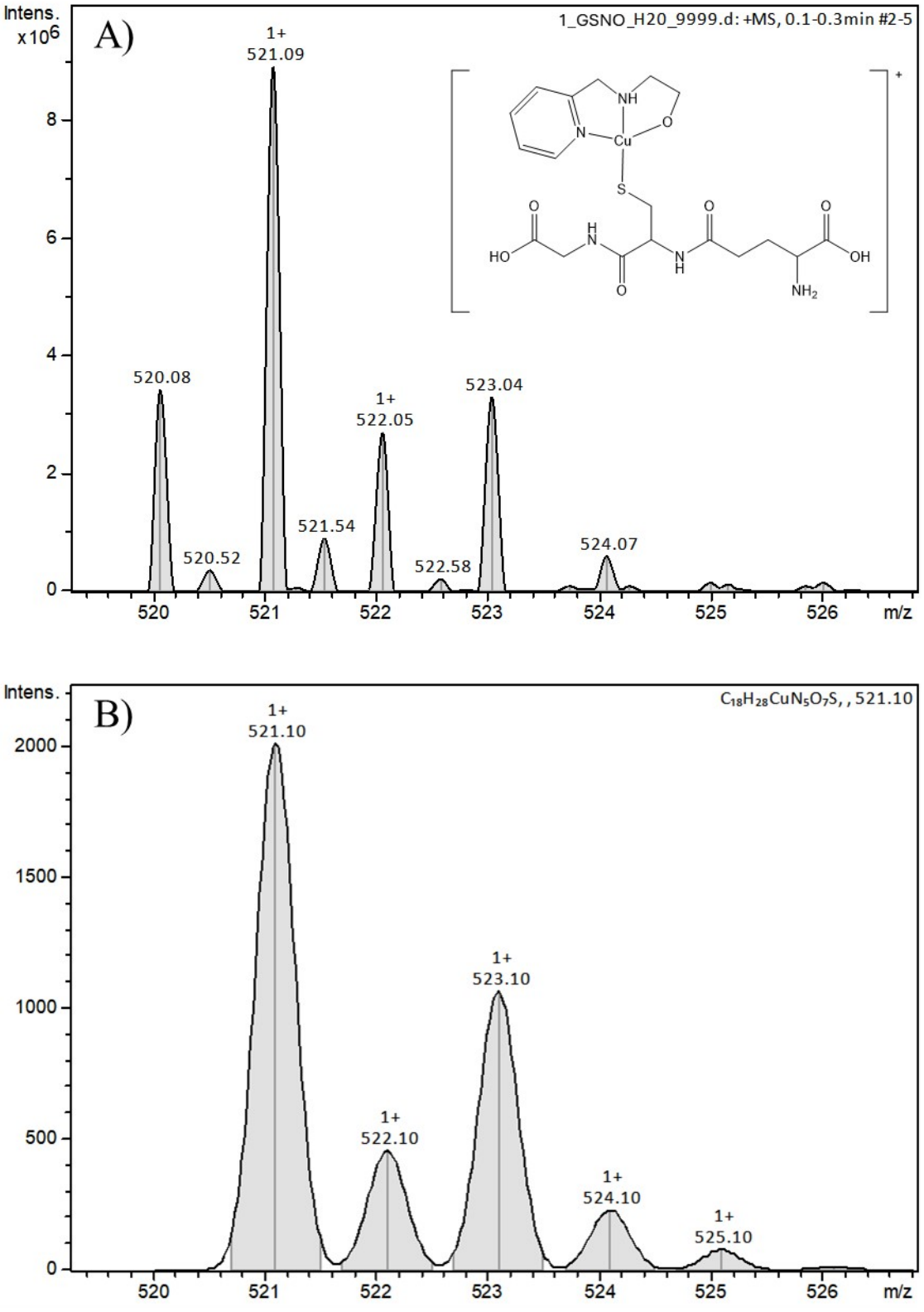

Figure 33S. Experimental and (b) simulated ESI-(+)-MS isotopic pattern of the fragment *m/z* 521.09, corresponding to the adduct formed between complex **1** and GS·: $[Cu(L)(GS)]^+$.

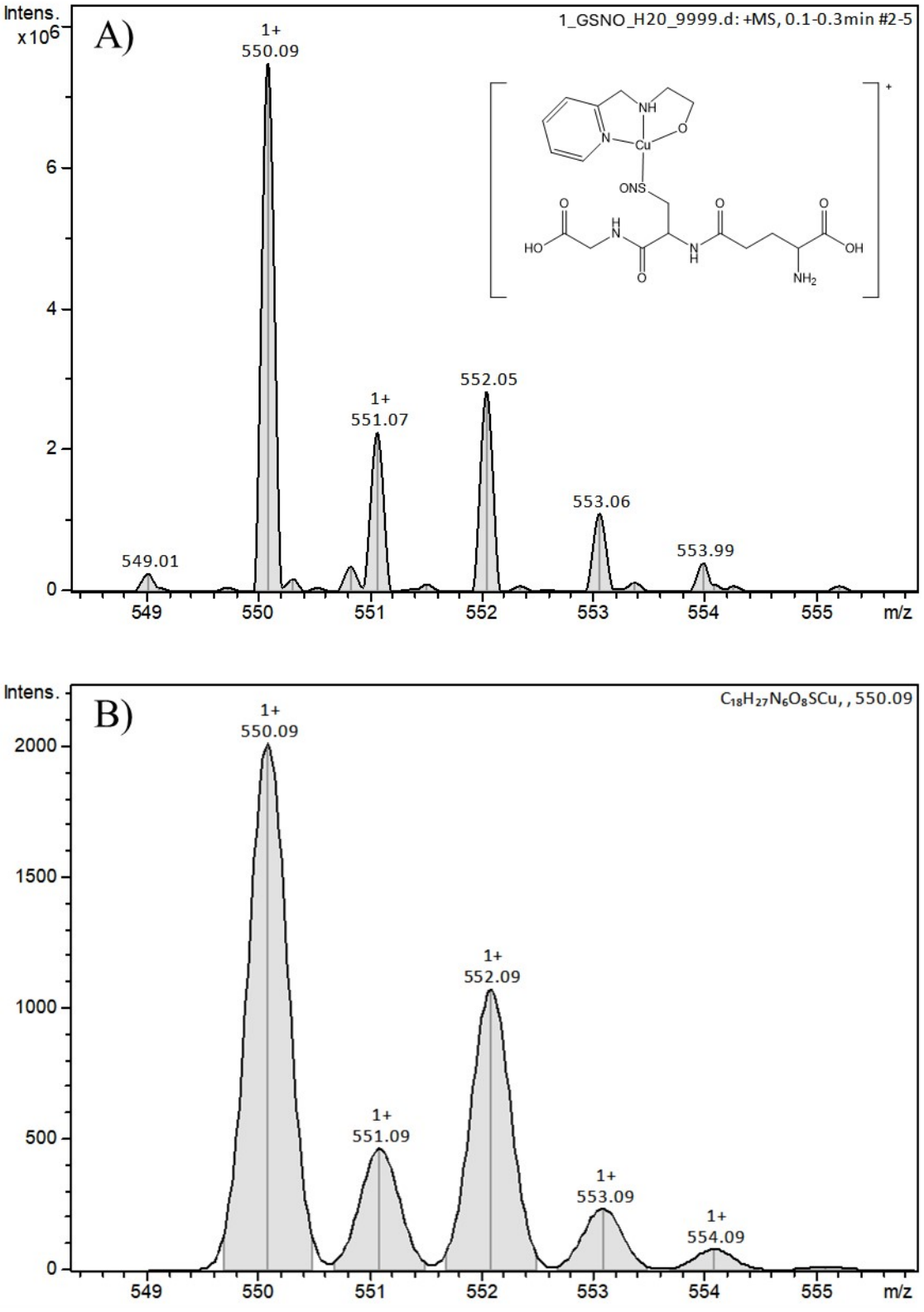

Figure 34S. Experimental and (b) simulated ESI-(+)-MS isotopic pattern of the fragment *m/z* 550.09, corresponding to the adduct formed between compound **1** and GSNO, in water: $[Cu(L)(GSNO)]^+$.

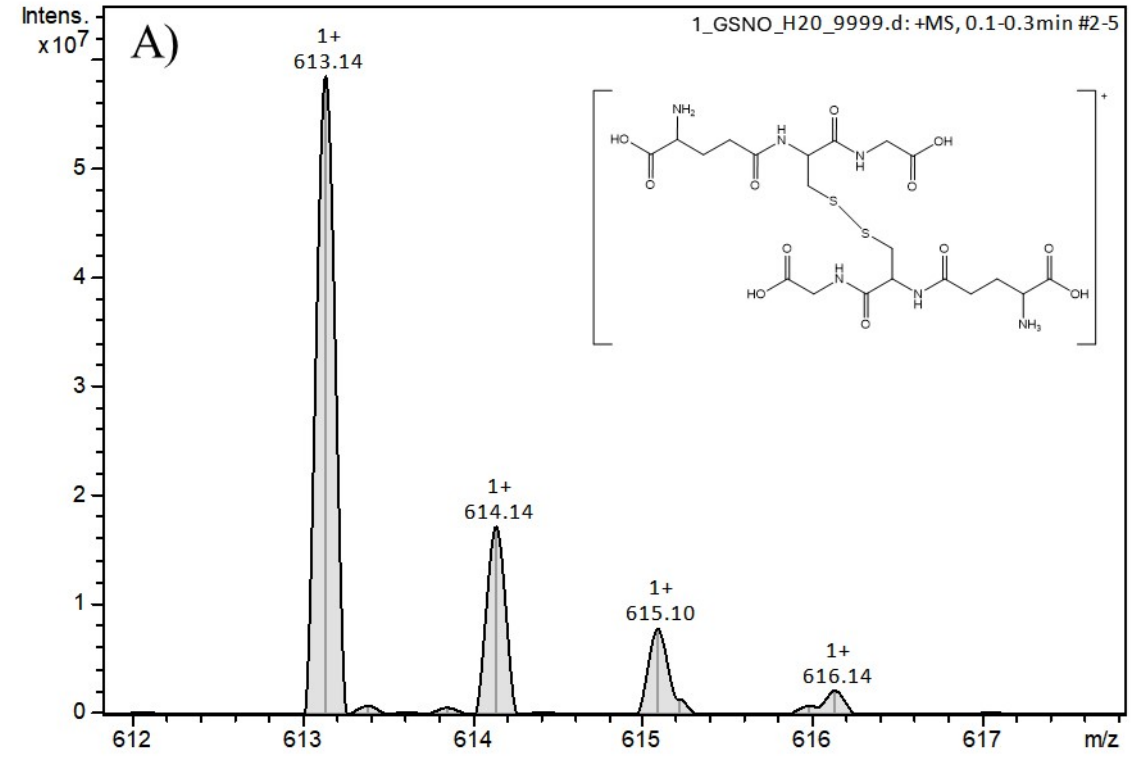

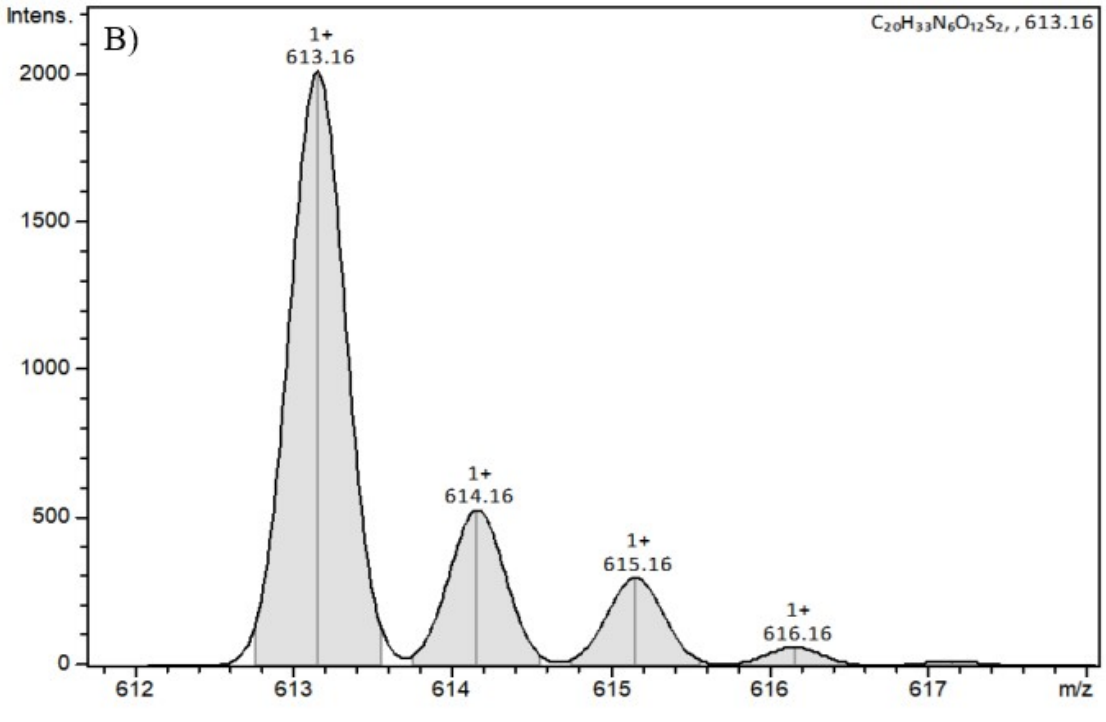

Figure 35S. Experimental and (b) simulated ESI-(+)-MS isotopic pattern of the fragment *m/z* 613.14, corresponding to the formation of the protonated species of the molecule GSSG: $[GSSG + H]^+$.

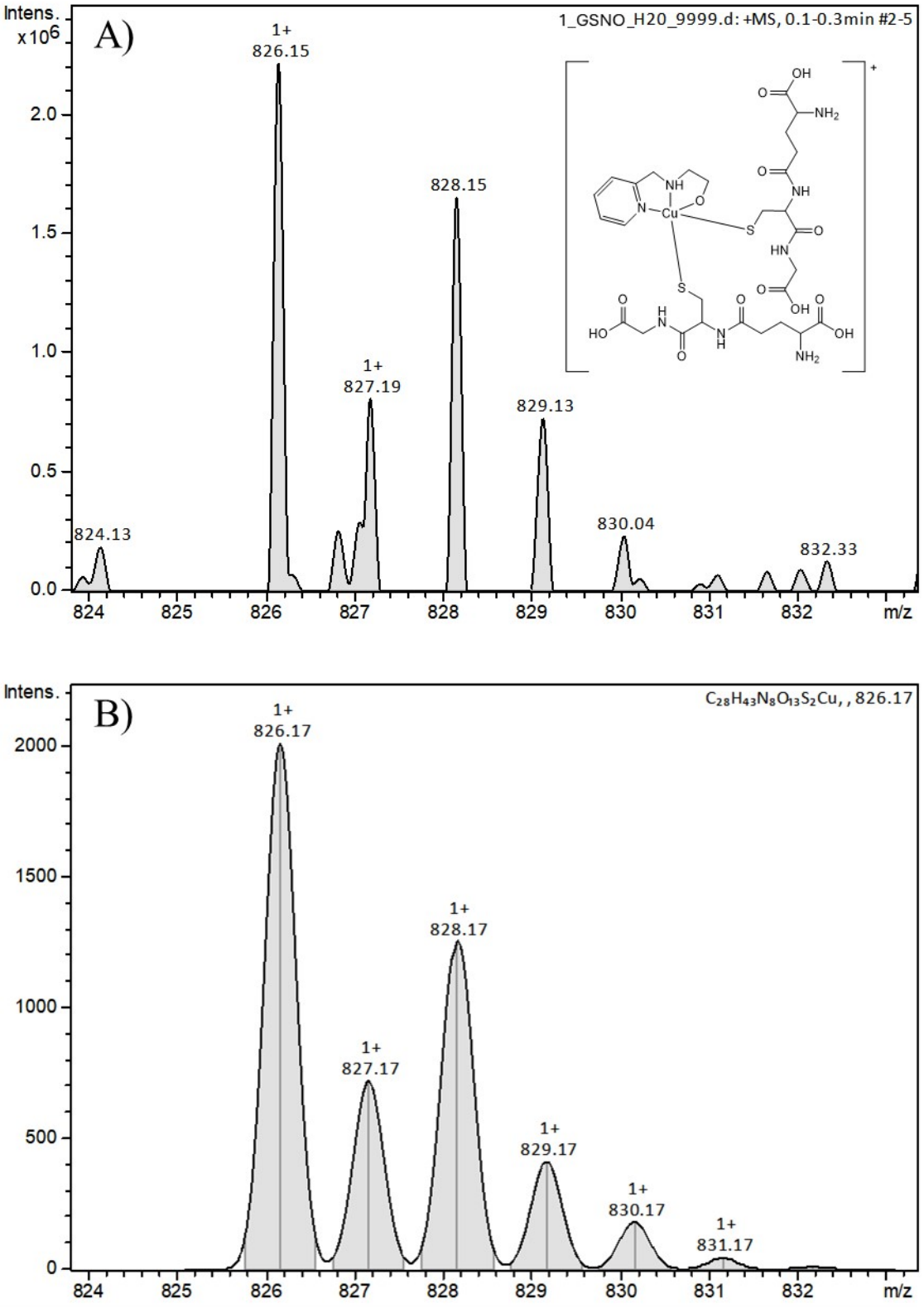

Figure 36S. Experimental and (b) simulated ESI-(+)-MS isotopic pattern of the fragment *m/z* 826.17, corresponding to the adduct formed between compound **1** and two molecules of GS·: $[Cu(L)(GS)_2]^+$.

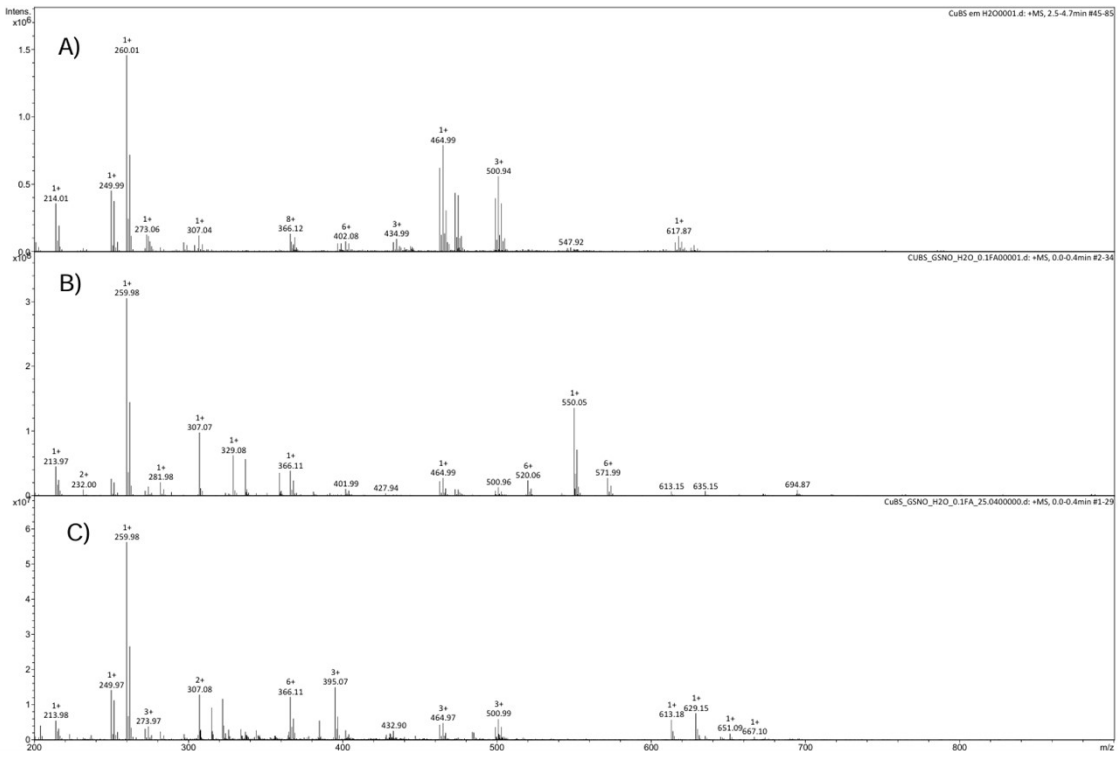

Figure 37S. Monitoring of the interaction between compound **1** and GSNO, by ESI-(+)-MS, in water: a) spectrum of compound **1**, and attribution for the main cations: $[Cu(HL)Cl]^+$ = *m/z* 249.98, $[Cu(HL)(formic\ acid)]^+$ = *m/z* 260.01, $[Cu(HL)(L)(H_2O)]^+$= *m/z* 464.99 b) spectrum obtained immediately after the interaction between compound **1** and GSNO, and attribution for the main cations: $[Cu(HL)Cl]^+$ *m/z* 249.98, $[Cu(HL)(formic\ acid)]^+$ *m/z* 260.01, $[Cu(HL)(L)(H_2O)]^+$*m/z* 464.99, $[GSH+H]^+$*m/z* 308.03, $[GSNO+H]^+$ *m/z* 338.02, $[Cu(L)(GS)]^+$ *m/z* 521.09, $[Cu(L)(GSNO)]^+$ *m/z* 550.09, $[GSSG + H]^+$ *m/z* 613.14. b) spectrum obtained 48h after the interaction between compound **1** and GSNO. Note the absence of the peak attributed to the cation $[Cu(L)(GSNO)]^+$ of *m/z* 550.09, in c), indicating that after 48h, all the GSNO was consumed.

S3.8. Quantification of •NO

The reaction chamber was filled with 11 mL of PBS buffer (0.01 mol L^{-1}) and kept at 37°C while the reaction mixture was continuously purged with either nitrogen or air. Using a Hamilton syringe, 10 µL of **1** (100 µmol L^{-1}; i.e. 1 µmole absolute) was added to

the reaction chamber, followed by the addition of 10 µL of GSNO (1 mmol L^{-1}; i.e. 10 µmoles). These data are presented in Figure 8 in the manuscript and in Figure 38S in the supplementary material.

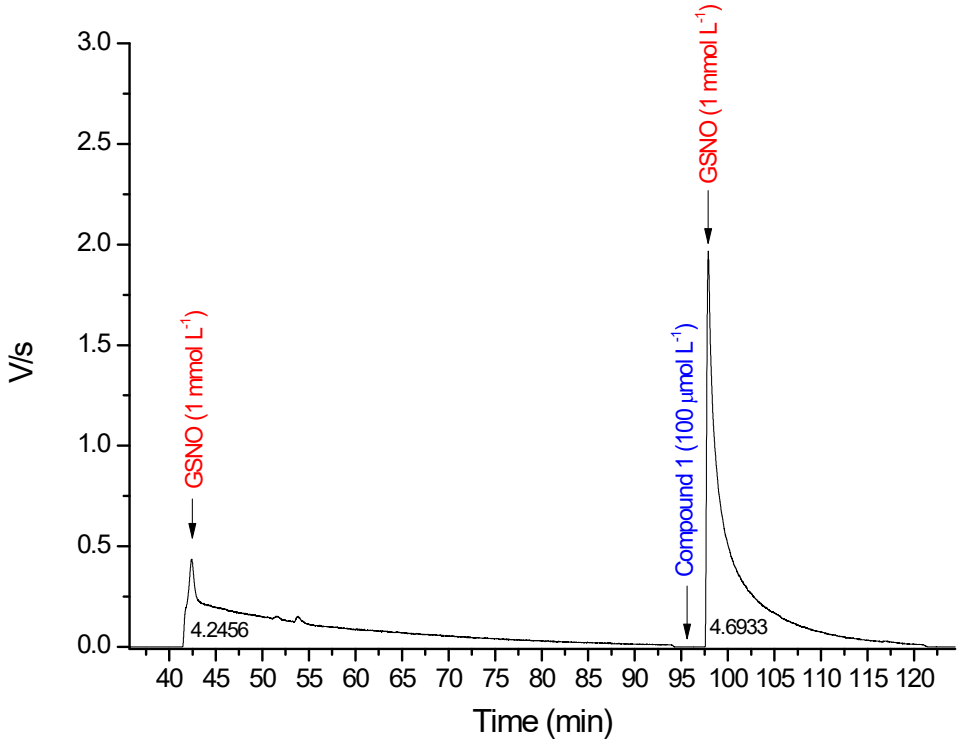

Figure 38S. GSNO decomposition monitored by CLD in the absence and presence of compound **1**. 20 µL of a **1** mmol L^{-1} solution of GSNO was added to a glass chamber containing 25 mL of PBS (integration value of peak: 4.2456). The chamber was washed three times with Mili-Q water then, 20 µL of a 100 µmol L^{-1} solution of compound **1** was added to the chamber, followed by the addition of 20 µL of a 1 mmol L^{-1} solution of GSNO (integration value of the peak: 4.6933)

S3.9- - Computational Details of the interaction between compound 1 and GSNO

The starting structure of compound **1** was built using the crystal structure of the compound reported herein. All calculations were performed using the Gaussian 16 software package.[9] All structures in the mechanism were optimized without any symmetry constraints at mpw1pw91[9]/LANL2DZ[10] level of theory utilizing the

Hay−Wadt effective core potentials[11] for Cu ions. The 6-31G*[12-14] basis set was used to treat C, H, N, and O atoms and 6-311G**[15] basis set to treat the S atom. All the Hessian calculations were also done with the same level of theory as used for optimization. The final energies were improved using a higher level of theory (mpw1pw91/LANL2TZ, [10, 16-20] for Cu and 6-311++G**[12,16] for all other atoms). The zero-point vibrational, thermal, and entropic corrections were included. The solvent effects were incorporated using the self-consistent reaction field-IEFPCM implicit solvent model.[21,22] All the structures exist in the doublet spin state.

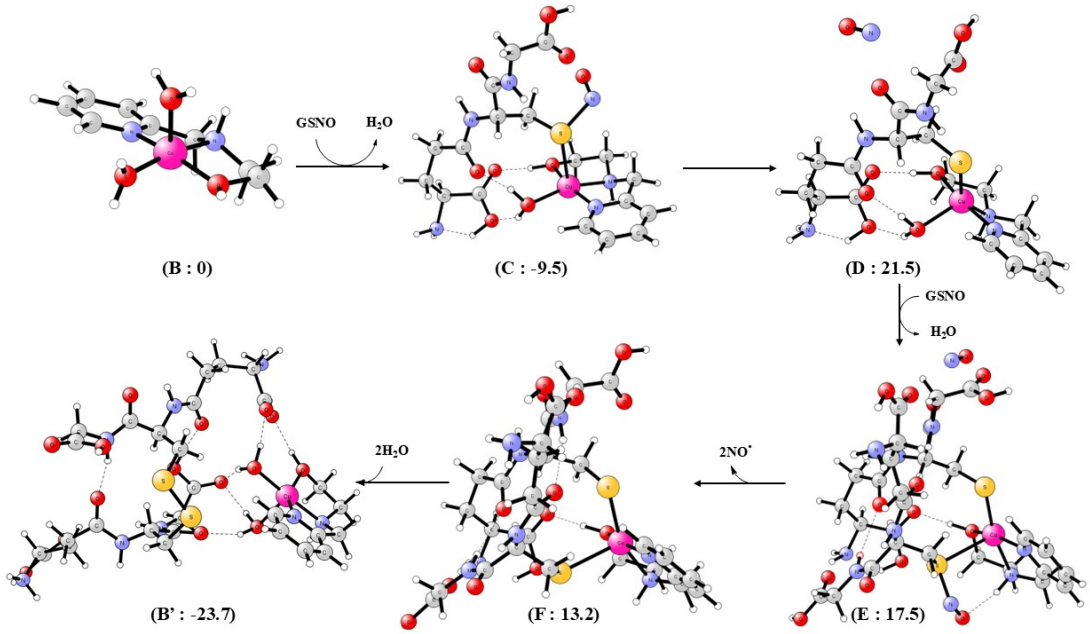

Figure 39S. Proposed mechanism for denitrosylation of GNSO, catalyzed by compound **1**, showing the stabilization of the structures by multiple hydrogen bonds. Gibb's free energies are shown in parentheses (kcal/mol) for species **B-E**, species **A** is the starting compound, in PBS: $[Cu(HL)(OH_2)_2]$.

SI references

(1) G. M. Sheldrick, Crystal structure refinement with SHELXL, *Acta Crystallogr C Struct Chem* **2015**, *71*, 3.

(2) G. M. Sheldrick, A short history of SHELX, *Acta Crystallogr A* **2008**, *64*, 112.

(3) K. Bradenburg, H. Putz, Diamond- Crystal and Molecular Structure Visualization (version 4.6.0). Crystal Impact GbR-Bonn, Germany, **2019**.

(4) C. Fernandes, A. Horn Jr., O.Vieira-da-Motta, M. M. Kanashiro et el. Synthesis, characterization, antibacterial and antitumoral activities of mononuclear zinc complexes containing tridentate amine-based ligands with N_3 or N_2O donor groups, *Inorg. Chim. Acta*. **2014**, *24*, 35.

(5) A. P. Cardoso, L. M. P. Madureira, B. B. Segat, J. do N. C. Menezes, R. Cargnelutti, D. R. S. Candela, D. L. Mariano, R. L. T. Parreira, A. Horn, S. H. Seabra, R. A. DaMatta, F. F. Moreira, R. V. Moreira, G. F. Caramori, C. Fernandes, Development, structural, spectroscopic and in silico investigation of new complexes relevant as anti-toxoplasma metallopharmacs, *J Mol Struct* **2022**, *1265*, 133380.

(6) C. Nunes, J. Laranjinha, Nitric oxide production from nitrite plus ascorbate during ischemia upon hippocampal glutamate NMDA receptor stimulation, *BioChem* **2023**, *3*, 78.

(7) Weiss JN. FASEB J. The Hill equation revisited: uses and misuses, **1997**,11(11), 835.

(8) S. Ghosh, P. Roy, S. Prasad, G. Mugesh, Crystal-facet-dependent denitrosylation: modulation of NO release from **S**-nitrosothiols by Cu2O polymorphs, *Chem Sci* **2019**, *10*, 5308.

(9) M. J. Frisch, G. W. Trucks, H. B. Schlegel, G. E. Scuseria, M. A. Robb, J. R. Cheeseman, G. Scalmani, V. Barone, G. A. Petersson, H. Nakatsuji, X. Li, M. Caricato, A. V. Marenich, J. Bloino, B. G. Janesko, R. Gomperts, B. Mennucci, H. P. Hratchian, J. V. Ortiz, A. F. Izmaylov, J. L. Sonnenberg, Williams, F. Ding, F. Lipparini, F. Egidi, J. Goings, B. Peng, A. Petrone, T. Henderson, D. Ranasinghe, V. G. Zakrzewski, J. Gao, N. Rega, G. Zheng, W. Liang, M. Hada, M. Ehara, K. Toyota, R. Fukuda, J. Hasegawa, M. Ishida, T. Nakajima, Y. Honda, O. Kitao, H. Nakai, T. Vreven, K. Throssell, J. A. Montgomery Jr., J. E. Peralta, F. Ogliaro, M. J. Bearpark, J. J. Heyd, E. N. Brothers, K. N. Kudin, V. N. Staroverov, T. A. Keith, R. Kobayashi, J. Normand, K. Raghavachari, A. P. Rendell, J. C. Burant, S. S. Iyengar, J. Tomasi, M. Cossi, J. M. Millam, M. Klene, C. Adamo, R. Cammi, J. W. Ochterski, R. L. ; Martin, K. Morokuma, O. Farkas, J. B. Foresman, D. J. Fox, 2016.

(10) C. Adamo, V. Barone, Exchange functionals with improved long-range behavior and adiabatic connection methods without adjustable parameters: The mPW and mPW1PW models, *J Chem Phys* **1998**, *108*, 664.

(11) P. J. Hay, W. R. Wadt, *Ab initio* effective core potentials for molecular calculations. Potentials for K to Au including the outermost core orbitals, *J Chem Phys* **1985**, *82*, 299.

(12) P. J. Hay, W. R. Wadt, Ab initio effective core potentials for molecular calculations. Potentials for the transition metal atoms Sc to Hg, *J Chem Phys* **1985**, *82*, 270.

(13) T. Clark, J. Chandrasekhar, G. W. Spitznagel, P. V. R. Schleyer, Efficient diffuse function-augmented basis sets for anion calculations. III. The 3-21+ G basis set for first-row elements, Li–F, *J Comput Chem* **1983**, *4*, 294.

(14) P. C. Hariharan, J.A. Pople, The influence of polarization functions on molecular orbital hydrogenation energies, *Theoret Chim Acta* **1973**, *28*, 213.

(15) W. J. Hehre, R. Ditchfield, J. A. Pople, Self—consistent molecular orbital methods. XII. Further extensions of Gaussian—type basis sets for use in molecular orbital studies of organic molecules, *J Chem Phys* **1972**, *56*, 2257.

(16) R. Krishnan, J. S. Binkley, R. Seeger, J. A. Pople, Self-consistent molecular orbital methods. XX. A basis set for correlated wave functions, *J Chem Phys* **1980**, *72*, 650.

(17) B. P. Pritchard, D. Altarawy, B. Didier, T. D. Gibson, T. L. Windus, New basis set exchange: An open, up-to-date resource for the molecular sciences community, *J Chem Inf Model* **2019**, *59*, 4814.

(18) D. Feller, The role of databases in support of computational chemistry calculations, *J Comput Chem* **1996**, *17* (13), 1571.

(19) K. L. Schuchardt, B. T. Didier, T. Elsethagen, L. Sun, V. Gurumoorthi, J. Chase, J. Li, T. L. Windus, Basis set exchange: a community database for computational sciences, *J. Chem. Inf. Model* **2007**, 47, 3, 1045.

(20) L. E. Roy, P. J. Hay, R. L. Martin, Revised basis sets for the LANL effective core potentials, *J Chem Theory Comput* **2008**, *4*, 1029.

(21) E. Cancès, B. Mennucci, J. Tomasi, A new integral equation formalism for the polarizable continuum model: Theoretical background and applications to isotropic and anisotropic dielectrics. *J. Chem. Phys.* **1997**, *107*, 3032.

(22) B. Mennucci, R. Cammi, J. Tomasi, Excited states and solvatochromic shifts within a nonequilibrium solvation approach: A new formulation of the integral equation formalism method at the self-consistent field, configuration interaction, and multiconfiguration self-consistent field level. *J. Chem. Phys.* **1998**, *109*, 2798.